AD/A-001 624

DESIGN AND FABRICATION OF STRIPLINE MICROWAVE SURFACE-CRACK DETECTOR FOR PROJECTILES

Ulrich H. Gysel, et al

Stanford Research Institute

Prepared for:

Army Materials and Mechanics Research Center

September 1974

DISTRIBUTED BY:

NTIS

National Technical Information Service
U. S. DEPARTMENT OF COMMERCE

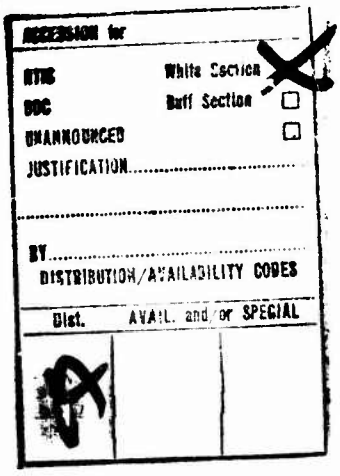

The findings in this report are not to be construed as an official Department of the Army position, unless so designated by other authorized documents.

Mention of any trade names or manufacturers in this report shall not be construed as advertising nor as an official indorsement or approval of such products or companies by the United States Government.

This project has been accomplished as part of the U.S. Army Materials Testing Technology Program, which has for its objective the timely establishment of testing techniques, procedures or prototype equipment (in mechanical, chemical, or nondestructive testing) to insure efficient inspection methods for materiel/material procured or maintained by AMC.

DISPOSITION INSTRUCTIONS

Destroy this report when it is no longer needed.
Do not return it to the originator.

UNCLASSIFIED

SECURITY CLASSIFICATION OF THIS PAGE (When Data Entered)

REPORT DOCUMENTATION PAGE

READ INSTRUCTIONS BEFORE COMPLETING FORM

1. REPORT NUMBER: AMMRC CTR 74-58 per ddc
2. GOVT ACCESSION NO.
3. RECIPIENT'S CATALOG NUMBER: AD/A-001 624

4. TITLE (and Subtitle): DESIGN AND FABRICATION OF STRIPLINE MICROWAVE SURFACE-CRACK DETECTOR FOR PROJECTILES

5. TYPE OF REPORT & PERIOD COVERED: Final Report Covering the Period 16 July 1973 to 15 July 1974

6. PERFORMING ORG. REPORT NUMBER: Final Report SRI Project 2821

7. AUTHOR(s): Ulrich H. Gysel and Lester Feinstein

8. CONTRACT OR GRANT NUMBER(s): DAAG46-73-C-0257

9. PERFORMING ORGANIZATION NAME AND ADDRESS: Stanford Research Institute, Menlo Park, California 94025

10. PROGRAM ELEMENT, PROJECT, TASK AREA & WORK UNIT NUMBERS: D/A Project-PEMA, AMCMS Code 5396-OM-6350

11. CONTROLLING OFFICE NAME AND ADDRESS: Army Materials and Mechanics Research Center, Watertown, Massachusetts 02172

12. REPORT DATE: September 1974

13. NO. OF PAGES: 91

14. MONITORING AGENCY NAME & ADDRESS (if diff. from Controlling Office)

15. SECURITY CLASS. (of this report): Unclassified

15a. DECLASSIFICATION/DOWNGRADING SCHEDULE: N/A

16. DISTRIBUTION STATEMENT (of this report)

Approved for public release; distribution unlimited.

17. DISTRIBUTION STATEMENT (of the abstract entered in Block 20, if different from report)

18. SUPPLEMENTARY NOTES

DDC RECEIVED DEC 3 1974 D

19. KEY WORDS (Continue on reverse side if necessary and identify by block number)

Nondestructive tests

Microwaves

Reproduced by NATIONAL TECHNICAL INFORMATION SERVICE U S Department of Commerce Springfield VA 22151

20. ABSTRACT (Continue on reverse side if necessary and identify by block number)

A self-contained coupled-stripline crack detector was built, tested, and evaluated. This detector makes use of the capability of two coupled striplines to support two orthogonal modes. The two conductors, printed on a dielectric sheet whose other side is clad with metal, scan the metal surface at a close distance. The metal surface then becomes part of the RF ground conductor. The two striplines are excited in one mode and a crack in the metal surface couples energy into the other mode, because the crack upsets the symmetry of the coupled lines. A complete

DD FORM 1 JAN 73 1473

EDITION OF 1 NOV 65 IS OBSOLETE

UNCLASSIFIED

SECURITY CLASSIFICATION OF THIS PAGE (When Data Entered)

19. KEY WORDS (Continued)

20 ABSTRACT (Continued)

detector system was built consisting of RF source, modulator, coupled-stripline detector with even-mode exciter and odd-mode receiver, and the necessary low-frequency amplifiers and detectors. Extensive measurements were performed with a planar detector on planar plates and a curved detector on 175-mm artillery shell bodies. The system operates at 10 GHz and has tuning adjustments to give better than 75 dB isolation between the two modes at the output of the stripline detector. Artificial cracks in a wide range of sizes were machined into the test objects. All were detected, with the smallest one being 0.0015 inch wide, 0.005 inch deep, and 0.1 inch long. A disadvantage of the present system that affects its sensitivity is the difficulty of maintaining high isolation between the two modes at the output of the detector. This is a result of changes in the spacing between the detector and the test object. Correlation techniques were also examined for capabilites that would further enhance the detection of cracks. Ways in which the detector system can be improved are discussed.

ABSTRACT

A self-contained coupled-stripline crack detector was built, tested, and evaluated. This detector makes use of the capability of two coupled striplines to support two orthogonal modes. The two conductors, printed on a dielectric sheet whose other side is clad with metal, scan the metal surface at a close distance. The metal surface then becomes part of the RF ground conductor. The two striplines are excited in one mode and a crack in the metal surface couples energy into the other mode, because the crack upsets the symmetry of the coupled lines. A complete detector system was built consisting of RF source, modulator, coupled-stripline detector with even-mode exciter and odd-mode receiver, and the necessary low-frequency amplifiers and detectors. Extensive measurements were performed with a planar detector on planar plates and a curved detector on 175-mm artillery shell bodies. The system operates at 10 GHz and has tuning adjustments to give better than 75 dB isolation between the two modes at the output of the stripline detector. Artificial cracks in a wide range of sizes were machined into the test objects. All were detected, with the smallest one being 0.0015 inch wide, 0.005 inch deep, and 0.1 inch long. A disadvantage of the present system that affects its sensitivity is the difficulty of maintaining high isolation between the two modes at the output of the detector. This is a result of changes in the spacing between the detector and the test object. Correlation techniques were also examined for capabilities that would further enhance the detection of cracks. Ways in which the detector system can be improved are discussed.

FOREWORD

The research covered in this report was performed with the direction and support of the Army Materials and Mechanics Research Center, Watertown, Massachusetts, under Contract DAAG46-73-C-0257. The technical supervisor was Mr. Otto Gericke.

The authors wish to thank Mr. York Sato of SRI who very ably fabricated and tested most of the system. Dr. Don Parker and Mr. Lloyd Robinson both of SRI participated in valuable discussions throughout the period of this work.

Preceding page blank

CONTENTS

Preceding page blank

ILLUSTRATIONS

TABLES

I INTRODUCTION

The principle of microwave detection of cracks in a metal surface was demonstrated by Hruby and Feinstein[1*] several years ago. They used the mode conversion that takes place when an electromagnetic wave of a given polarization impinges on a planar metal surface with a crack. In the practical experiment a dual-mode waveguide horn antenna was utilized to illuminate the surface and receive the reflected wave. This horn antenna illuminated an area about 2 cm in diameter. Mechanical scanning in two directions was required to cover the total area of interest.

In the search for a scanner that examines a larger area than a horn at any instant, a strip-transmission-line detector was developed by Robinson and Gysel.[2] The principle of operation is again based on the mode conversion that takes place when a crack disrupts the fields that are set up by the exciting mode. Because of the linear extension of the stripline crack detector, one single scan is sufficient to scan an area. In the previous work[2] the theoretical foundations for a stripline crack detector were developed. This led to an optimum geometry for the detector. An experimental detector proved the principle of operation, but it was far from a practical instrument.

This report presents the results of an extension of the initial work on the stripline crack detector. The goals of the latest research effort were threefold. Firstly, a self-contained system suitable to test a realistic object such as the 175-mm artillery shell body was to be built. Secondly, extensive measurements were to be performed and

---

*References are listed at the end of the report.

the sensitivity limits of the new system were to be established. Finally, various signal-processing techniques that would enhance the detection capabilities of the basic system were to be explored. All three goals were fully achieved and their respective limitations determined.

II THEORY OF COUPLED-STRIPLINE CRACK DETECTOR

A. Principle of Operation

A brief introduction to the principle of operation of the stripline crack detector is presented in this section. It is a shortened version of the detailed treatment that can be found in the original work by Robinson and Gysel.[2]

The basic effect that permits the stripline crack detector to detect cracks is that the crack supplies a coupling mechanism between two modes that are naturally decoupled--i.e., orthogonal. The input microwave signal excites only one mode, and the detector couples only to the other mode. The choice of modes was such that any asymmetry, such as a surface crack, couples power between the modes. By the use of orthogonal modes, a sensitive system was built. In the absence of surface cracks, the system is balanced so that no signal, or very little, reaches the detector. When a crack unbalances the system, a small but measurable signal reaches the detector and is displayed on the indicator device. The system can also be considered to be a bridge arrangement.

A stripline structure that can support two orthogonal TEM modes is a pair of coupled strips, for which the cross-section geometry, the electric fields, and the currents are shown in Figure 1. The direction of propagation is perpendicular to the plane of the figure. For the even mode, illustrated in Figure 1(a), the two strips are at the same potential with respect to ground. When the strips are of equal width, as will be assumed here, they carry equal currents in the same direction. The return currents in the ground planes are, of course, in a direction opposite to the strip currents. For the odd mode, illustrated in

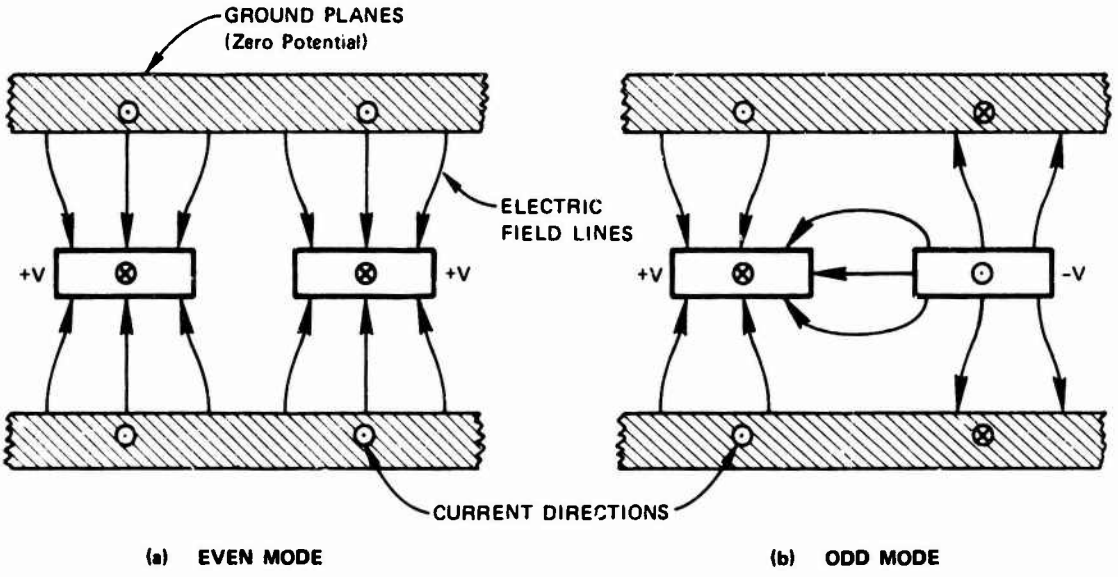

FIGURE 1 TWO ORTHOGONAL MODES FOR A PAIR OF COUPLED STRIPLINES
(support dielectric not shown)

Figure 1(b), the two strips have potentials, with respect to ground, of the same magnitudes, but of opposite polarities. The strips carry opposite but equal currents. Note that the two ground-plane currents shown also flow in opposite directions.

When the pair of strips is excited in the even mode there will be no conversion to the odd mode as long as symmetry is maintained. However, when a surface crack in one ground plane perturbs the current under one strip but not the other, some power is converted to the odd mode. The incident-mode current excites the crack, which can then be thought of as a virtual current generator required to satisfy the local boundary conditions. The crack-induced current does not have either type of symmetry shown in Figure 1, so it will excite both modes. Of particular interest is the coupling to the odd mode. The detector

circuitry was made sensitive only to the odd mode, and thus can indicate the presence of a crack.*

B. Selection of a Suitable Stripline Cross Section

Of primary importance for the operation of the stripline crack detector is the current distribution for the even mode and the odd mode on the ground-plane conductor, which eventually will be formed by the surface of the test specimen. Figure 2, which is reproduced here for ease of reference from Ref. 2, shows a typical cross section and the two current distributions. The parameters of this stripline geometry are the width, w, of each of the two strips, the separation, s, between the strips, the distance, a, between the strips and the surface being examined, the thickness, b, of the dielectric supporting the strips, and the relative dielectric constant, ε_r, of the support dielectric.

The current distributions for the stripline cross section shown in Figure 2 are plotted to the same horizontal scale as for the cross section at the top of the figure. The curve of even-mode current has even symmetry about the plane of mechanical symmetry ($x = 0$), and the curve of odd-mode current has odd symmetry about $x = 0$. For both modes in this example, the ground-plane current reaches a maximum within the width of the strip conductor, and falls off rapidly at positions outside the strip ($|x/s| > 3.68$ on the figure). Between the strips ($|x/s| < 0.5$

---

*The crack-induced current will also couple to a third mode, the parallel-plate mode. This mode has an electric field extending from one ground plane to the other, just as if the strips were not present. This mode was suppressed by lossy material located away from the strips. This parallel-plate mode is not useful for indicating the presence of a crack because the connections from the striplines to the generator and to the detector also excite some parallel-plate mode. To avoid higher-order stripline modes, the spacing between ground planes is only a fraction of a wavelength.

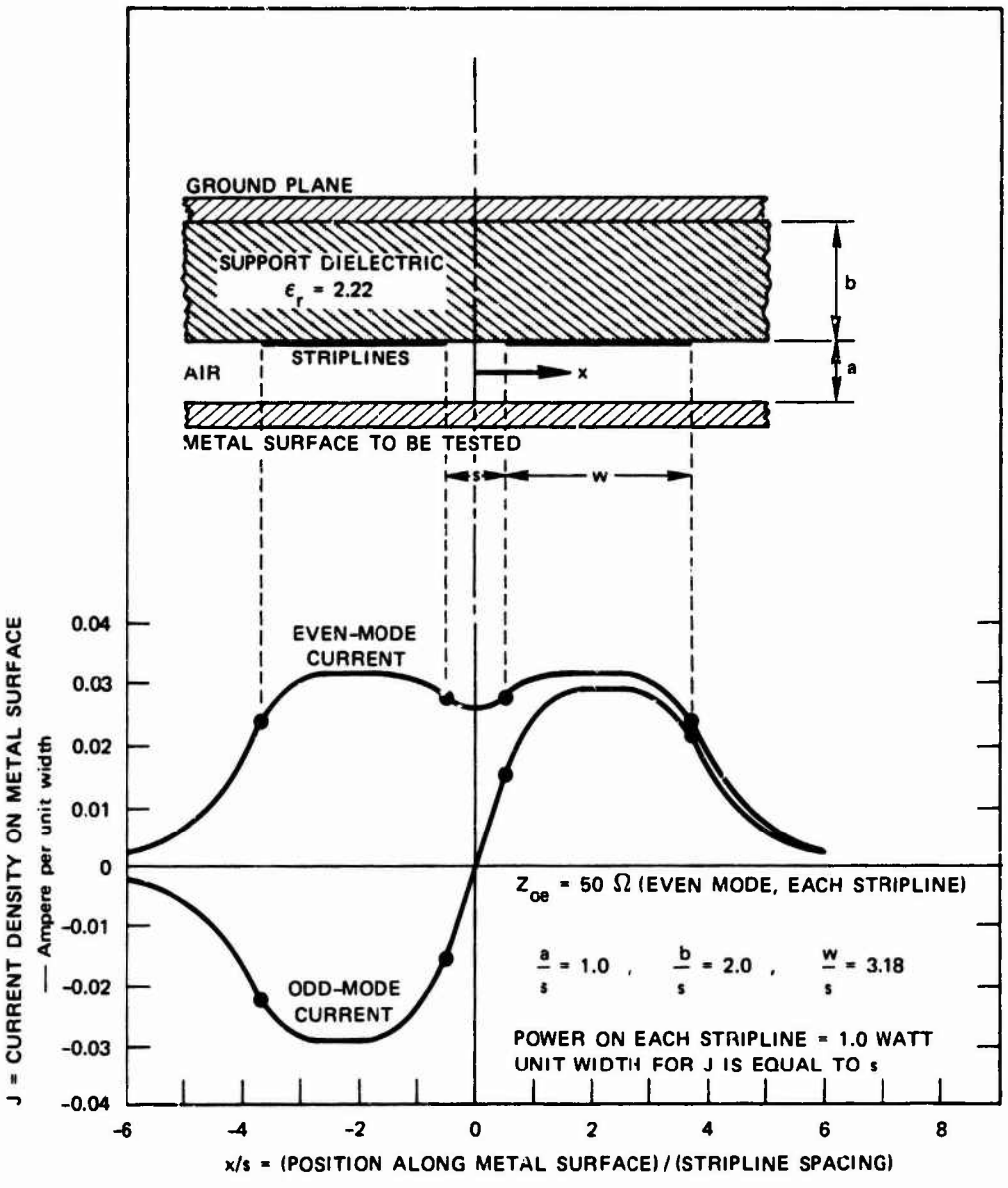

FIGURE 2 SURFACE-CURRENT DISTRIBUTION FOR EVEN AND ODD MODES OF THE COUPLED STRIPLINES

on Figure 2), the even-mode current on the ground plane is only slightly less than its peak value, but the odd-mode current goes to zero at x = 0 because of the reversal in current direction for negative x. (For the sake of generality, all theoretical curves have dimensions normalized to the stripline spacing, s.

It will be shown below that the sensitivity of the detector is directly proportional to the product of the current densities of the even and odd mode. These current densities can be maximized principally by minimizing the ratios a/b and a/s. However, a number of constraints set lower limits to these ratios. A few factors are mentioned in the following. One of the constraints on these variables is the impedance of the crack-detector system which should be reasonably close to 50 ohms so that it can be matched to available generators and detectors. Another constraint is that the cross-section dimensions be small enough compared to the operating wavelength that higher-order modes do not propagate.[3] Such modes could produce spurious responses that interfere with operation of the crack detector. Small cross-sectional dimensions are also required to get good resolution for cracks in the x direction.

However, mechanical tolerances determine the smallest practical spacing between the striplines and the test surface. For the present detector the cross section, as shown in Figure 2, with a = 0.031 inch, was selected. This is the same cross section that was used in the previous work, where a detailed discussion of the various factors influencing the choice can be found.[2] To summarize those results, one can say that the chosen cross section has 92% of the sensitivity of uncoupled lines, small extension in the x direction, and is easy to match (Z_{oe} = 50 Ω, Z_{oo} = 42 Ω).

C. Sensitivity Analysis

In the crack-detector application, only the even mode is excited on the striplines by the generator. The detector circuitry is made sensitive only to the odd mode, and thus has zero output as long as symmetry is maintained. A small crack at a distance x from the plane of symmetry of the stripline couples power into the odd mode. The basic relationship on which this crack detector operates is that the amplitude of the crack-coupled signal is proportional to the current density of the even mode at the crack location if the generator and detector were interchanged.[4] Thus, the parameter of greatest interest here is the product of the even- and odd-mode current densities as a function of distance x from the plane of symmetry. The coupled signal amplitude is proportional to this product times a polarizability constant[4] that is a function of the crack length, width, and depth.

In the following we will calculate the coupled-signal amplitude for the simplified case of a crack perpendicular to the stripline axis and small in length compared with the width of the striplines. Also, to simplify the analysis, we assume that the two striplines numbered 1 and 2 are uncoupled. We assume now that a crack of known dimensions is located directly under Stripline 1. This crack can be replaced in an equivalent circuit by a small inductor with the reactance j2X in series with Stripline 1, as shown in Figure 3(a). Stripline 2 in undisturbed and no inductor is present in its equivalent circuit. The operation of the crack detector is best understood by analyzing even and odd modes on the two-line system. Applying the even- and odd-mode analysis to the circuit of Figure 3(a), the circuit of Figure 3(b) results. The crack under Stripline 1 has the effect of coupling the even- and odd-mode

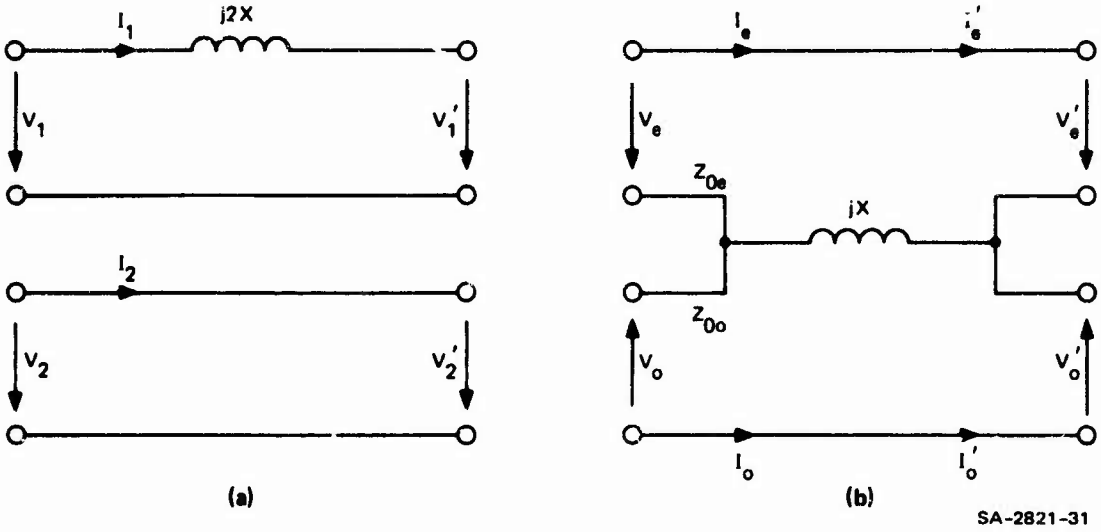

FIGURE 3 EQUIVALENT CIRCUIT FOR THE COUPLING EFFECT OF A CRACK IN A TWO-STRIPLINE SYSTEM

lines through a common series inductor with the reactance jX.* Analytically, this can be shown very easily. If the even- and odd-mode voltages and currents are expressed in terms of the direct line parameters, one obtains

$$V_e = \frac{1}{2}(V_1 + V_2) \qquad V_e' = \frac{1}{2}(V_1' + V_2')$$
$$V_o = \frac{1}{2}(V_1 - V_2) \qquad V_o' = \frac{1}{2}(V_1' - V_2') \tag{1}$$

and

$$I_e = \frac{1}{2}(I_1 + I_2)$$
$$I_o = \frac{1}{2}(I_1 - I_2) \quad . \tag{2}$$

*The schematic of Figure 3(b) is also that of two waveguides coupled through a hole in a common broad wall.[5] The only difference between the stripline crack detector and the waveguide coupler is the interchange of direct-equivalent circuit and even- and odd-mode circuit. For the waveguide coupler, Figure 3(a) represents the even- and odd-mode equivalent circuit, whereas Figure 3(b) corresponds to the direct-equivalent circuit.

For the circuit of Figure 3(a) we obtain the relations

$$V_1 = I_1 j2X + V_1'$$
$$V_2 = V_2' \quad . \tag{3}$$

Substituting Eq. (3) into Eq. (1) and expressing I_1 in terms of I_e and I_o, we obtain

$$V_e = (I_e + I_o)jX + V_e'$$
$$V_o = (I_e + I_o)jX + V_o' \tag{4}$$

which is exactly the system of equations that describes the circuit of Figure 3(b).

Our next step is to evaluate the reactance 2X of the inductor in Figure 3(a) that models a crack of a given length ℓ, width w, and depth d. The energy stored in the inductor is equal to the magnetic energy, W_m, stored in the crack. We assume as a first-order approximation that the magnetic field strength in the crack is the same as that on the undisturbed surface at the location of the crack, or

$$W_m = \frac{H_c^2}{2} \mu_0 \Delta V = \frac{\mu_0 J_c^2}{2} \Delta V \tag{5}$$

where

H_c = Magnetic field at the crack location

J_c = Surface current density at the crack location of the undisturbed line

ΔV = Volume of crack.

Now, W_m will be equated with the reactance X of the equivalent inductor:

$$2X = \omega\mu_0 \Delta V \frac{J_c^2}{\hat{I}_1^2} \tag{6}$$

where ω = radian frequency of operation. This expression can be simplified by use of the equality

$$\omega\mu_0 = 2\pi \frac{Z}{\lambda} \tag{7}$$

where

Z = Free-space wave impedance = 376.7 ohms

λ = Free-space wavelength.

Combining Eqs. (6) and (7), we obtain

$$X = \pi Z \left(\frac{J_c}{\hat{I}_1}\right)^2 \frac{\Delta V}{\lambda} \quad . \tag{8}$$

The quantity $J_c^2/\hat{I}_1^2$ can be determined from Figure 2. The error induced by doing that is small, even though Figure 2 shows the current densities in the test surface for slightly coupled transmission lines, whereas our example assumed completely uncoupled lines. From the figure we determine J_c = 0.03A/(unit width) in the area centered under the stripline. Taking the normalization of Figure 2 into account, we can express Eq. (8) as

$$X = \pi Z \left(\frac{0.03}{0.2}\right)^2 \frac{w}{s} \cdot \frac{d}{s} \cdot \frac{\ell}{\lambda} \quad . \tag{9}$$

The coupling between the even and odd mode that is caused by a crack with the equivalent reactance X can be readily calculated from Figure 3(b):

$$C = \frac{-jX/Z_0}{2(1 + jX/Z_0)} \qquad (10)$$

with Z_0 equal to the characteristic impedance of the striplines.

The following is a sample calculation of the coupling of a crack:

$$\ell = d = s = 0.031 \text{ inch}$$

$$w = 0.010 \text{ inch}$$

$$\lambda = 1.18 \text{ inch } (f = 10 \text{ GHz})$$

$$Z_0 = 50 \text{ ohms}$$

$$X/Z_0 = 2.66 \cdot 10^{-3}$$

$$C = 1.33 \cdot 10^{-3} \hat{=} -57.6 \text{ dB.}$$

This calculated coupling factor is well within the measurement range of our system, as will be shown later. In the measurement section we will show further that the calculated coupling factors agree very well with the observed results, thereby indicating that the presented analysis is applicable.

D. Detector Response for Perturbations of Finite Size

So far, the assumption was made that the physical extension of a perturbation in the test surface (e.g., a crack) is small in the x direction compared with the size of the coupled striplines. In practice, however, cracks that are much larger than the total width of the coupled striplines will be encountered. Therefore, further consideration must be given to the influence of different types of surface perturbations on the output signal of the detector. Fundamental to this study is the

inherent response of the stripline detector to a point disturbance, which was found to be proportional to the product of the even- and odd-mode current densities in the test surface. This response is shown in Figure 4(a) as the function s(x), where x is again the distance measured perpendicular to the stripline axis from the center between the two striplines. In order to simplify the following analysis, we have to find a simple measure for a perturbation of finite size. In the previous section we showed that a small crack stores additional magnetic energy and that the detector output is proportional to this stored energy (or proportional to an equivalent inductor). Similarly, a small ridge or bump on the test surface can be considered as a source for additional stored electric energy, and the detector output is again proportional to this stored energy.

In a straightforward extension of the concept of stored energy, we assign a finite perturbation the function $p(\hat{x})$, where $\hat{x}$ is the measure along the x-axis with respct to some reference point along the perturbation. The function $p(\hat{x})$ is defined to represent the total stored energy of the perturbation between the distance $\hat{x}$ and $\hat{x} + d\hat{x}$. As a first approximation, the cross section of the perturbation at the point $\hat{x}$, measured in a plane perpendicular to the x-axis and with respect to a perfectly flat surface, will be a good approximation for $p(\hat{x})$. Therefore, a positive value for $p(\hat{x})$ would be assigned to a bump or a ridge, whereas a crack would be assigned a negative value. The position of the perturbation with respect to the coupled striplines is defined by the x-coordinate of its reference point, χ. Figure 4(a) shows, as an example, a triangularly shaped perturbation. In the x-coordinate system the perturbation is given by the function $p(x - \chi)$. The output signal of the detector for a given position χ of the perturbation can be found by integrating the contributions from small elements of length dx along the length of the perturbation, or

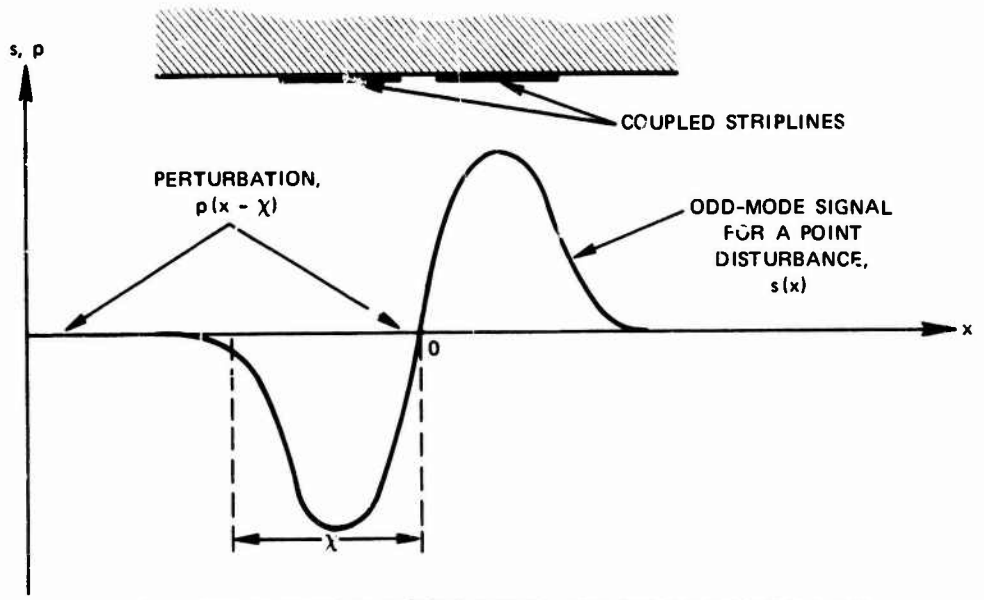

(a) CHARACTERISTIC OUTPUT SIGNAL AND SAMPLE PERTURBATION

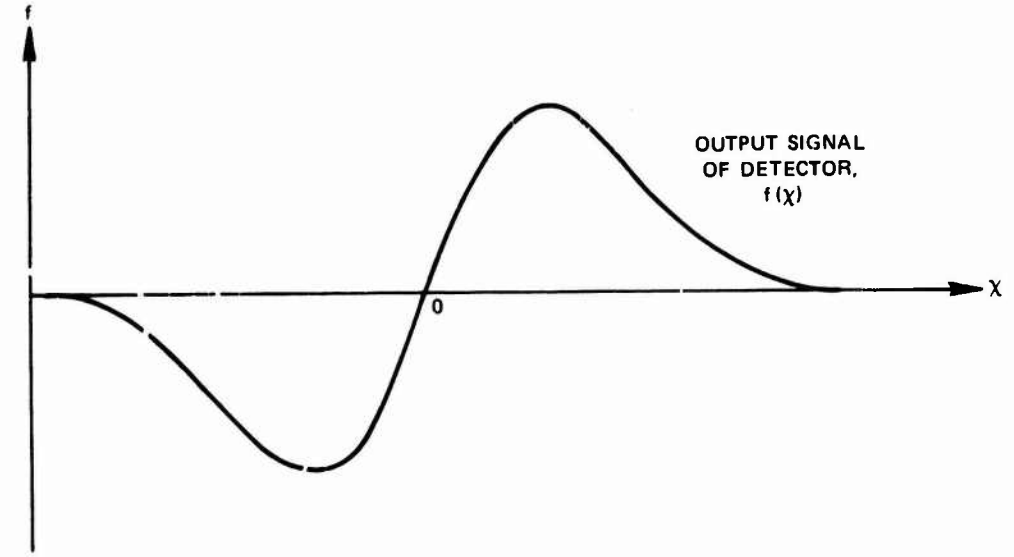

(b) OUTPUT SIGNAL OF DETECTOR f(χ)

SA-2821-10

FIGURE 4 OUTPUT SIGNAL FOR A FINITE PERTURBATION

$$f(\chi) = \int_{-\infty}^{\infty} s(x)\ p(x - \chi)dx \quad . \qquad (11)$$

This equation has the functional form of a convolution. If the perturbation is scanned by the detector, the function $f(\chi)$ is the waveform that will be observed as a function of the scanned distance, χ. Figure 4(b) is a plot of the result of Eq. (11) for the sample perturbation of Figure 4(a).

From this analysis it becomes obvious that perturbations small in length compared with the stripline size will lead to an output waveform, which reflects the inherent response of the detector, s(x). For larger perturbations the response gets smeared out, and for functions of $p(\hat{x})$ that vary very slowly compared with s(x), the output signal will ultimately disappear. A special case exists for a long perturbation that has a constant value for $p(\hat{x})$ over its full length and the value zero outside. This could be a long crack of constant depth that starts and ends abruptly. If the length of this perturbation is much greater than the extent of the two coupled striplines in the x direction, the function s(x) appears to be convolved with a step function, as the leading edge of the perturbation passes the detector. As the detector further scans such a perturbation, the detector will cover a section where $p(\hat{x})$ is nonzero but constant and the integral of Eq. (11) will give a value zero because of the odd character of s(x). Eventually the trailing step will be convolved with s(x). Now the convolution between s(x) and a step function is equal to the integral of s(x). Therefore the function $f(\chi)$ for a long, but constant perturbation will be a pulse equal to the integral of s(x) centered about the leading edge of the perturbation. The same pulse but of opposite polarity (assuming that the system is phase-sensitive) will appear centered about the trailing edge. The

important theoretical conclusion is that the leading edges of the signal tell essentially whether the perturbation has an abrupt step or starts more gradually. This conclusion is believed to hold true even in cases where the characteristic signal shown in Figure 4 gets distorted, as will be shown in the experimental part. There we will see that the theoretically calculated response $f(\chi)$ will be found only rarely. But the theoretical results derived in this section are essential for the interpretation of the measured responses.

III DESIGN AND CONSTRUCTION OF A CURVED STRIPLINE CRACK DETECTOR

A. System Design

A major step in the construction of the improved crack detector was the evaluation and selection of a suitable system. The major factors that were considered are performance, flexibility, and cost. The major performance factor is the sensitivity of the RF system--i.e., the smallest odd-mode RF signal that can be detected. Next, it was considered essential that the system be flexible enough to be interchangeable with different types of stripline detectors (e.g., planar and curved detectors). Finally, it was decided that wherever their performance was acceptable, commercial components should be utilized. This approach offers a price and time advantage over an all-in-house development. The system that was eventually selected is shown in Figure 5. A detailed description and a sensitivity analysis of this system follow.

The RF-source is a Gunn oscillator with 50 mW output power. The frequency is tunable mechanically from 9.2 to 10.4 GHz. The oscillator is followed by a 3-dB attenuator and a first power divider which splits the input power into equal parts. Half of the power is then directed to the quadrature IF mixer. The other half of the RF power passes an isolator and a SPDT switch that square-wave modulates the RF signal at 1 kHz. One output port of the switch is terminated in a load, whereas the second one is connected to a second power divider. For the proper operation of the system, it is absolutely important that the LO signal for the quadrature IF mixer is constant and does not contain any modulated components. Even though the system utilizes a single-pole,

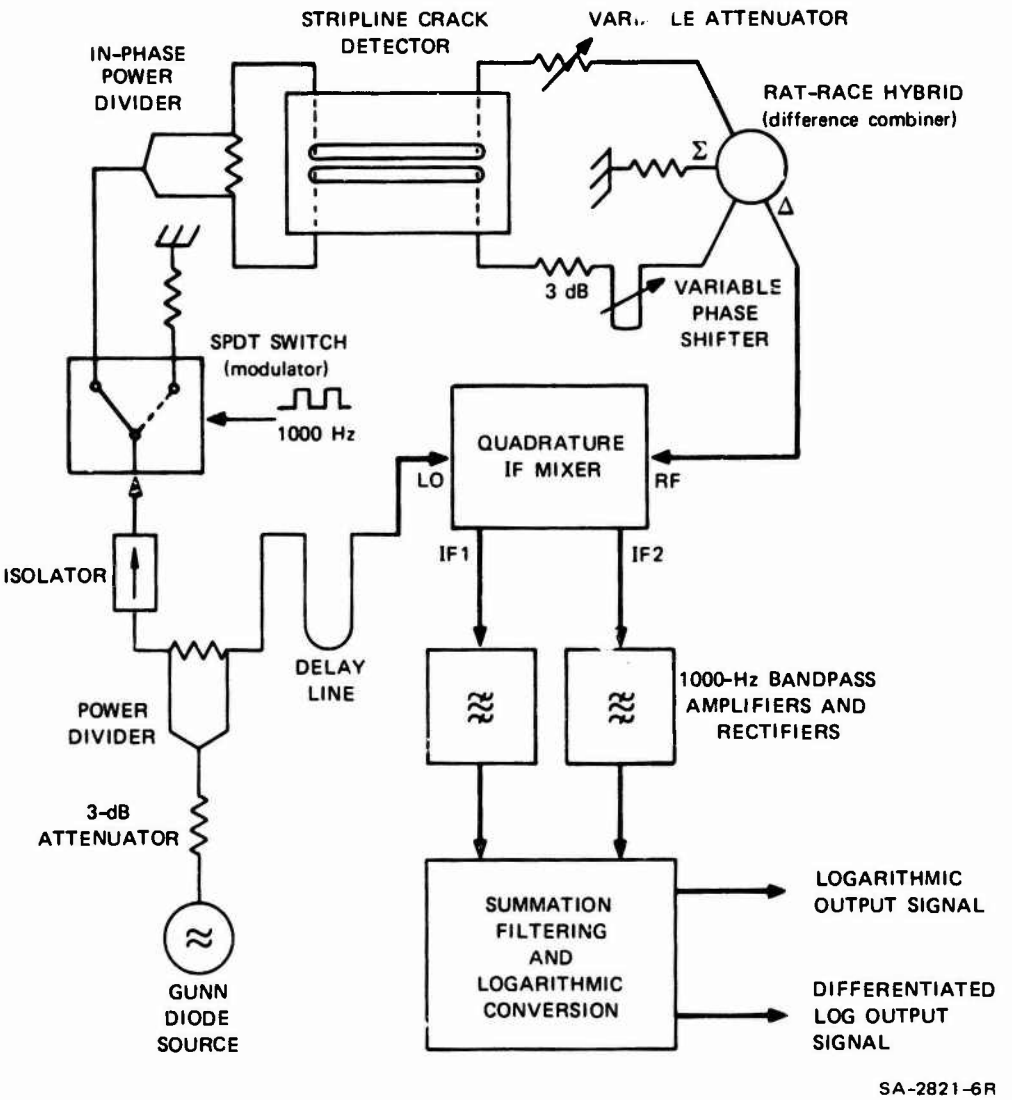

FIGURE 5 FINAL SYSTEM FOR COUPLED-STRIPLINE SURFACE-CRACK DETECTOR

double-throw switch, which represents a match at the input port in both switch positions as opposed to a single-pole, single-throw switch, the small differences in the input VSWR between the two switch positions are reflected back toward the oscillator. The power divider together with the 3-dB attenuator in front of it, produce at least 20 dB of isolation between the two output ports of the divider. However, it was found necessary to install an isolator with more than 40 dB isolation to sufficiently eliminate any modulated components in the LO signal.

The second power divider that follows the modulator excites the even mode on the coupled stripline detector because the two signals emerging from the power divider are equal and in phase. At the output of the detector, the difference port of a rat-race hybrid (180° hybrid or magic Tee) detects the odd-mode signal. The even-mode signal from the striplines is terminated by the load on the sum port of the hybrid. Tuning of the stripline detector for maximum decoupling between the even- and odd-mode components occurs with a variable attenuator in one branch leading from the detector to the rat-race hybrid and a fixed 3-dB attenuator and a variable phase shifter in the other branch. This combination permits tuning out of any remaining unbalances of the detector, when the detector is placed on a reference surface (e.g., perfectly smooth surface).

The difference (odd-mode output) port of the rat-race hybrid is connected to the RF port of a quadrature IF mixer, as shown in Figure 5. A quadrature IF mixer consists of two balanced mixers. Each of these receives half of the total RF input signal that is split in an in-phase power divider. The total LO oscillator is also divided equally in amplitude between the two mixers; however, division is accomplished with a 3-dB quadrature hybrid, resulting in 90° phase shift of the two output signals. Therefore, the two IF output signals of a quadrature IF mixer will always be 90° out of phase. This is very important in the

present application, because the LO and RF signal are at the same frequency, leading to a dc IF signal. Whenever the RF and LO signal are 90° out of phase, the output of a single balanced mixer will be zero. In a quadrature IF mixer, the RF signal is also mixed with the LO signal shifted by 90°, and the LO signal would then be in phase with the RF signal. The two IF outputs of the quadrature IF mixer are quadrature components of the RF signal with respect to the LO signal. The delay line in the LO path of the mixer was added in order to make the electrical path length for the RF and LO signal about the same. Without this delay line, the phase shift between the LO and the RF signal changes very rapidly as a function of frequency. Minimizing of this phase shift was found to improve the tunability of the detector.

Each IF output of the mixer consists of two components, the rectified LO signal and the down-converted RF signal, which is squarewave-modulated with 1 kHz. Because of this modulation, the downconverted RF signal can easily be picked up with a 1-kHz bandpass amplifier, which thereby rejects the rectified LO signal. The two amplified 1-kHz signals will be rectified, added, and filtered. A logarithmic amplifier converts the linear output signal into a logarithmic signal, which is much easier to display because of the large dynamic range. The logarithmic output signal is further differentiated by means of a high-pass filter. The purpose of this operation is explained in Section IV-B. A detailed description of the low-frequency electronics is given in Section III-D.

The sensitivity of the receiver determines ultimately the sensitivity of the crack detector. Table 1 shows a power-budget analysis of the crack-detector system of Figure 5. Absolute power levels are expressed in dBm (dB with respect to a level of 1 mW). The power output of the Gunn oscillator is 50 mW or +17 dBm. Most of the transmission losses are self explanatory. The loss observed from the input to one of the two outputs of the second power divider does not appear in the table,

Table 1

POWER BUDGET OF CRACK-DETECTOR SYSTEM

Prime RF power available		+ 17 dBm
Losses in the signal path		
3 dB attenuator (two)	6 dB	
Isolator	2 dB	
Power divider	3.5 dB	
SPDT switch	1.5 dB	
Stripline-detector launching losses	4 dB	
Phase-shifter losses	1 dB	
Cable and stripline losses (measured for the curved detector)	15 dB	
Total losses		- 33 dB
Even-mode power level at rat-race sum port		- 16 dBm
Sensitivity of receiver (40 Hz bandwidth)		-110 dBm
Dynamic range		94 dB

because it is compensated by the recombination of the two even-mode signals in the rat-race hybrid. The stripline-detector launching losses and the cable and stripline losses represent average measured values. Although the mixer noise figure is usually determined by the conversion loss of the mixer, in this case it is determined instead by the much larger noise contribution from the rectified Gunn oscillator. Typically, the AM noise of a Gunn oscillator lies 120 dB below the carrier in a 100-Hz band centered 1 kHz off the carrier. The LO power at the input of each balanced mixer in the quadrature IF mixer is +6 dBm. Therefore,

the rectified LO noise at each IF output in a 40-Hz band around 1 kHz is -117 dBm. An additional factor of 7 dB signal-loss accounts for the fact that the LO noise contribution is continuous whereas the RF signal is quarewave-modulated and only the fundamental components of the squarewave signals are extracted. Hence, the resulting sensitivity of the receiver is -110 dBm. The dynamic range (i.e., the maximum difference between the even- and odd-mode signal, also called the decoupling)* that the system should be capable of measuring is 94 dB. This is sufficient dynamic range, in view of the expected decoupling as obtained from the sensitivity analysis of Section II-C. Measured data on the actual dynamic range are given in Section III-E.

Flexibility was maintained by building the system from individual components. Particularly, the stripline detectors were constructed as separate units. This allowed us to test the detector system initially with a planar detector and later replace the planar detector with a curved detector with minimum changes in the RF system.

With the exception of the rat-race hybrid, the variable phase shifter, and of course the stripline detector, all RF components were commercial units.

B. Construction of a Planar Stripline Detector

Initially, a planar detector was built with two objectives in mind: (1) to test a new design, and (2) to have a detector available

---

*The terms "coupling" and "decoupling" are used interchangeably. The only difference between the two is a change in sign, if expressed in dB. "Decoupling" is preferred when the system is being described, whereas "coupling" is better for describing the effect of a crack.

for tests of the detector system, thereby allowing more time for the design of a curved stripline detector.

The primary objective in designing the improved planar detector was to eliminate the choke system that was employed in the previous detector model.[2] This choke system very effectively shorted the RF ground plane of the crack detector and the test surface. But it was impractical to realize, particularly for a curved surface. The new detector, as shown in Figure 6, uses absorptive material that completely surrounds the coupled stripline portion. The major advantage of the new design is the absence of any absorptive material or of a choke system between the test surface and the circuit board; this eliminates any critical contact or gap between the detector and the test surface. Semi-rigid cables are connected to the four ports of the coupled striplines on the side opposite the one that will be exposed to the test surface. The four transitions from stripline to coaxial cable are designed to give low reflection coefficients.

The way the absorptive material suppresses any unwanted mode will now be briefly explained. A wave incident on any of the four ports will excite waves in a large number of propagation modes in order to fulfill the boundary conditions that exist for the field equations. One mode is the desired quasi-TEM mode that travels along the striplines, and is similar to a coaxial-line mode.[6] Another major component will be a mode called the parallel-plate mode.[7] This mode does not require a center conductor as a coaxial TEM mode does. Rather, it is a waveguide mode propagating from the point of excitation in all directions. By surrounding the coupled striplines with an efficient absorber for electromagnetic waves, this parallel-plate mode will be essentially damped out within about a wavelength. Because the quasi-TEM mode is confined to the immediate vicinity of the striplines where no absorptive material is present, it will be transmitted with losses that are determined

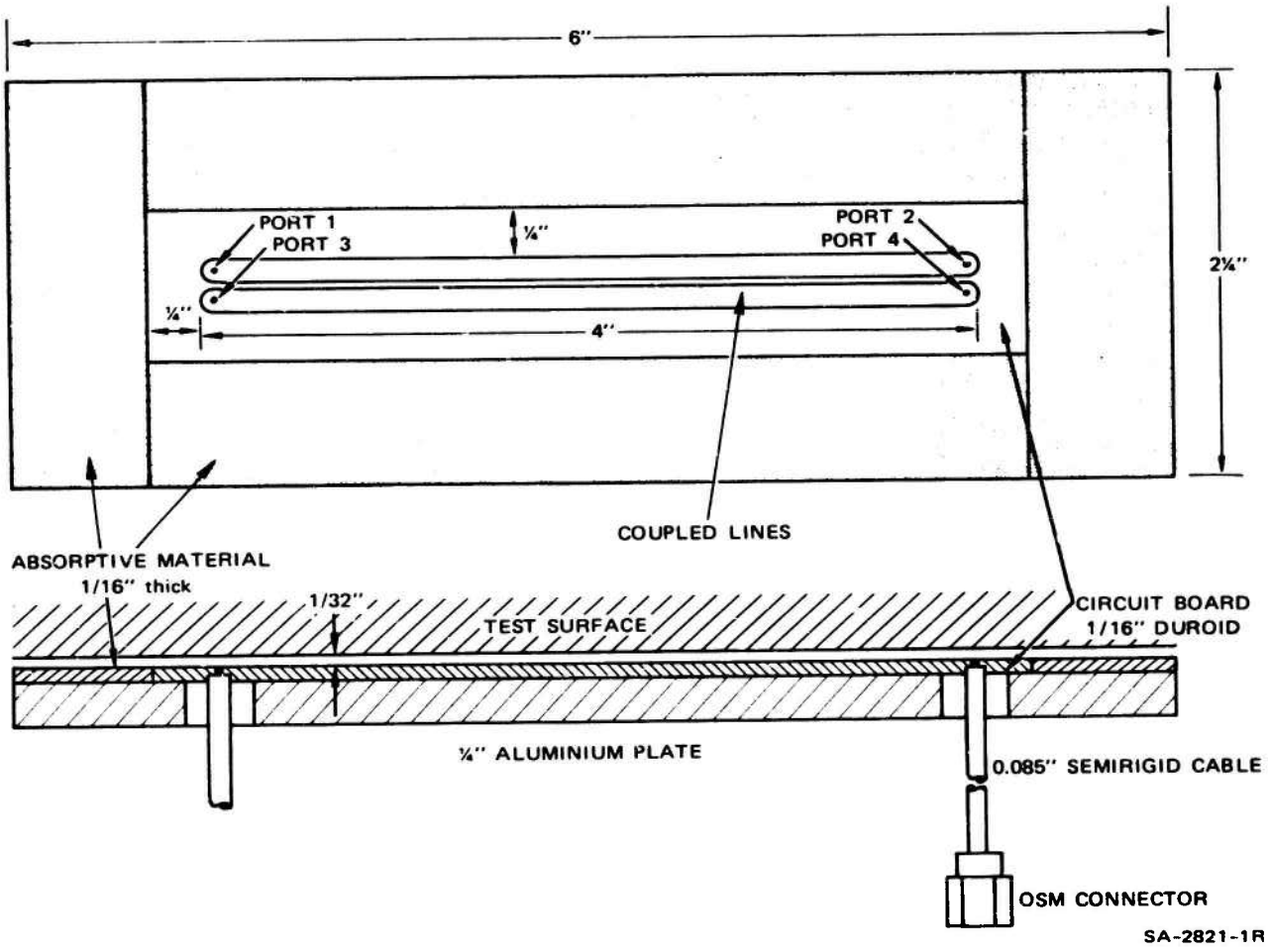

FIGURE 6 MECHANICAL DESIGN OF IMPROVED STRIPLINE CRACK DETECTOR

only by the losses of the circuit board and the conductivity of the test surface. However, due to the energy absorbed in all the unwanted modes, each transition from coaxial line to stripline has a conversion loss associated with it. If half the initial energy incident on the coaxial line were converted into the quasi-TEM mode, each transition would inherently contribute a loss of 3 dB.

The improved planar detector was initially tested as a directional coupler. This mode of operation does not correspond to that in the actual application, but is useful in evaluation of the new coaxial-to-stripline transition. Test results are shown in Figure 7. The input reflections on all ports are very low. At most ports and over most of the 9-to-11-GHz band, the return loss is below 15 dB.* If a signal is fed into Port 1, almost no energy is transmitted to Port 3. The amounts transmitted to Ports 2 ($|S_{21}|$) and 4 ($|S_{41}|$) are plotted in Figure 7. This mode of operation, in which Port 3 is isolated from Port 1, can be explained by the length of the coupled-line sections and the inhomogeneous dielectric medium surrounding the coupled lines. We are interested here only in the total energy transmitted to any of the other ports. At 10 GHz, 43% of the power is transmitted to Ports 2 and 4 together. Because in each of these paths two conversions had to take place, the conversion loss of one transition has to be less than 1.8 dB (no ohmic loss along the lines counted). This conversion loss is small and does not affect the overall sensitivity of the system as shown in Section III-A.

---

*The return loss is defined as $-20 \log |r|$, where r is the reflection coefficient. A return loss of 15 dB corresponds to a VSWR of 1.43.

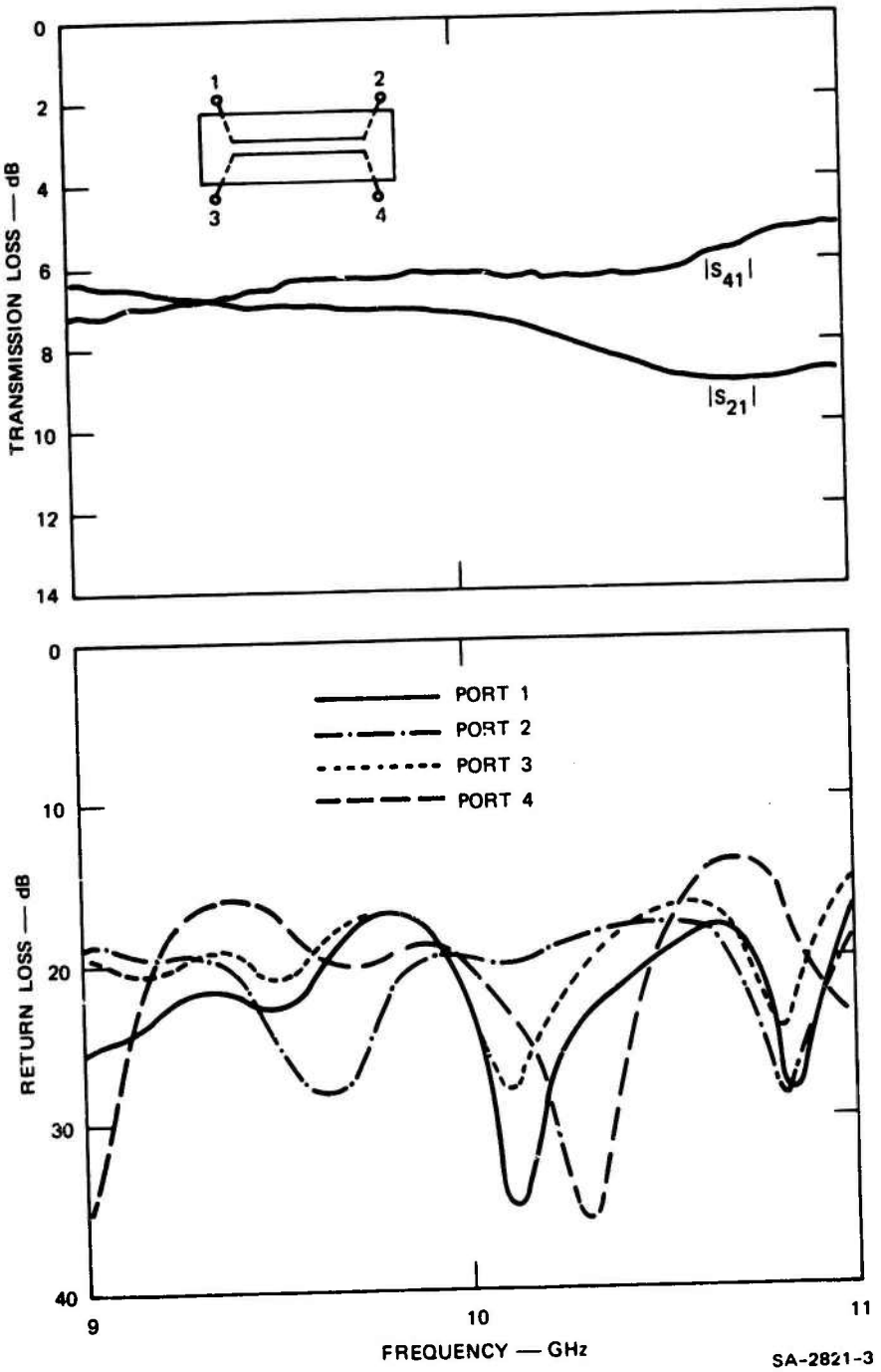

FIGURE 7 MEASURED RETURN LOSS AND TRANSMISSION LOSS OF IMPROVED STRIPLINE CRACK DETECTOR

C. Construction of a Curved Detector

After initial tests with the planar crack detector had demonstrated the effectiveness of the system, the step to a curved detector suitable for testing curved surfaces was small and involved mainly some constructional details. A cross section through the coupled striplines perpendicular to their axis is shown in Figure 8. The finished detector is

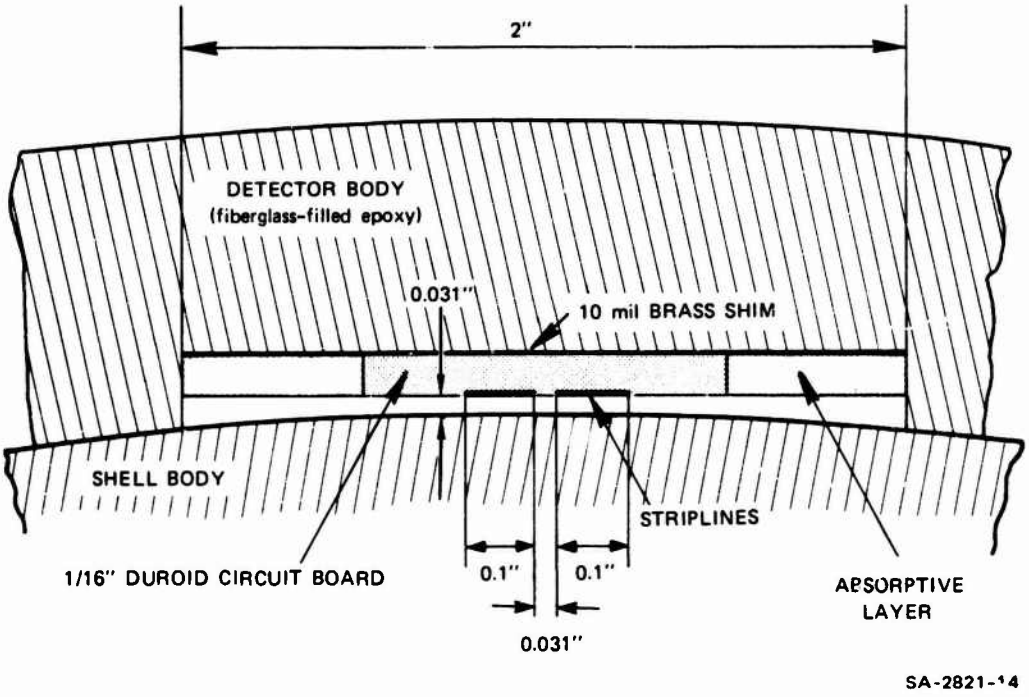

FIGURE 8 CROSS SECTION OF CURVED STRIPLINE CRACK DETECTOR

depicted in the photograph of Figure 9. The construction of this curved detector is essentially the same as the planar one. The two coupled striplines are printed on a 1/16-inch Duroid circuit board of 0.75 inch total width. On either side of the circuit board is a 0.625-inch-wide strip of absorptive material. A 10-mil brass shim provides the necessary conductive wall in those areas where the absorptive material is located.

SA 2821 23

FIGURE 9 CURVED CRACK DETECTOR, COUPLED-STRIPLINE SIDE

For the construction of the detector, the circuit board and the brass backing plate were soldered together while mounted on one of the shells, which served as a mold. The 31-mil gap between the detector and the shell as well as the space for the absorptive material were filled with teflon during that part of the construction. Then semirigid cables were soldered to the striplines. With the stripline assembly again mounted on the shell, the fiberglass-filled epoxy housing was formed. Eventually a chassis-plate was attached to the epoxy housing. The chassis plate carries the complete RF system, eliminating any RF cables between the stripline detector and a remotely located instrument box. Figure 10 shows the completed RF system.

To test the shells, a lathe was adapted to hold the 175-mm artillery-shell bodies. The detector is fixed in its axial position by means of the carriage of the lathe. The large contact area between the shell and the epoxy housing of the detector provides the necessary precision in guiding the detector on top of the rotating shell. Friction between the two parts is minimal due to the good sliding characteristics of epoxy. A photograph of the detector mounted on a shell is shown in Figure 11.

D. Low-Frequency Processing Electronics

The basic functions of the low-frequency processing electronics have been briefly discussed in Section III-A. In this section, a more detailed description is given. Detailed circuit diagrams are contained in the Appendix. The quadrature IF mixer furnishes two signals, each consisting of a dc component, which is due to the rectified LO signal and the down-converted RF component (a 1-kHz squarewave signal). Only the two 1-kHz components that represent quadrature components of the desired odd-mode signal are of any interest. They are processed

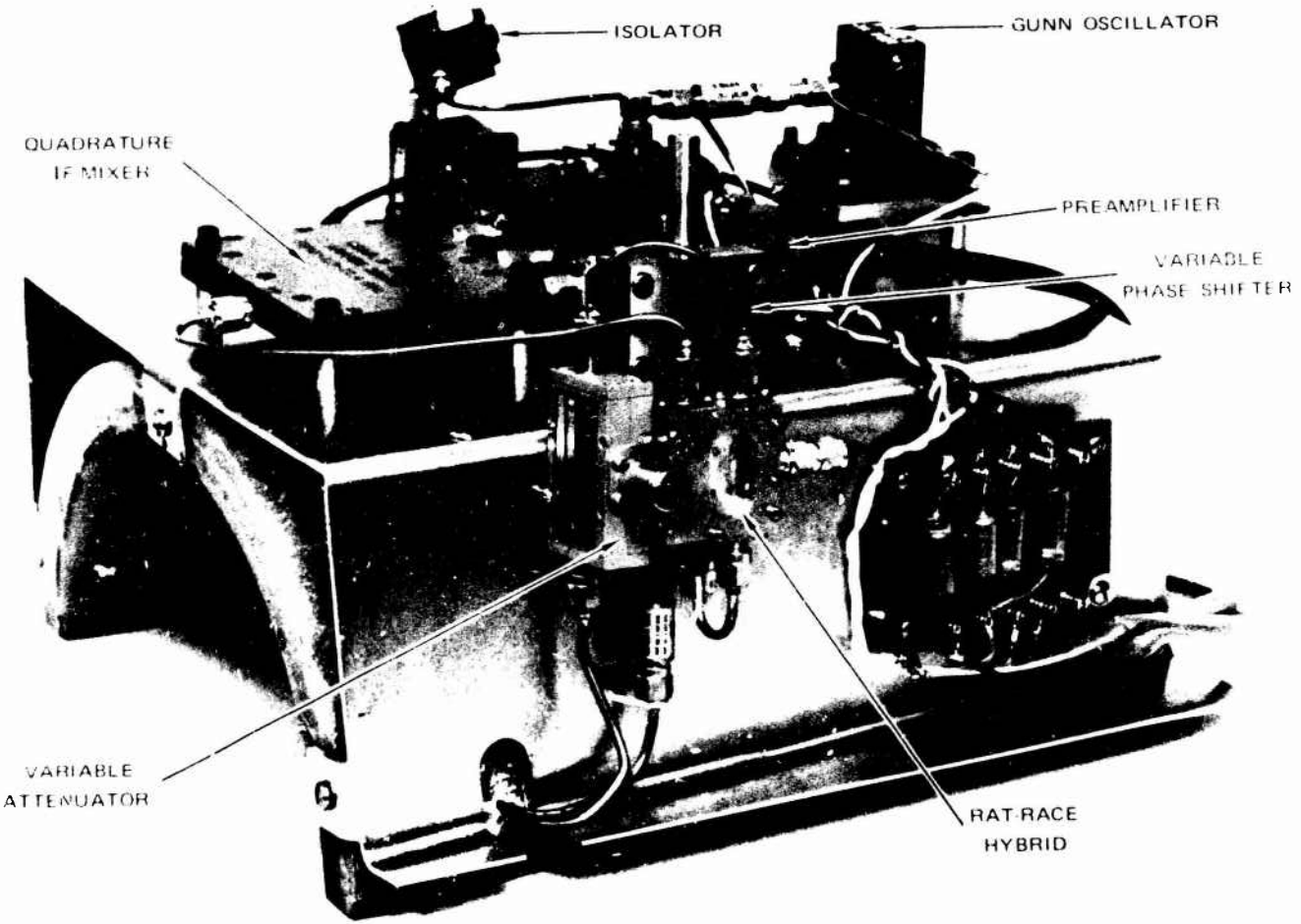

FIGURE 10 CURVED CRACK-DETECTOR SYSTEM, RF PART

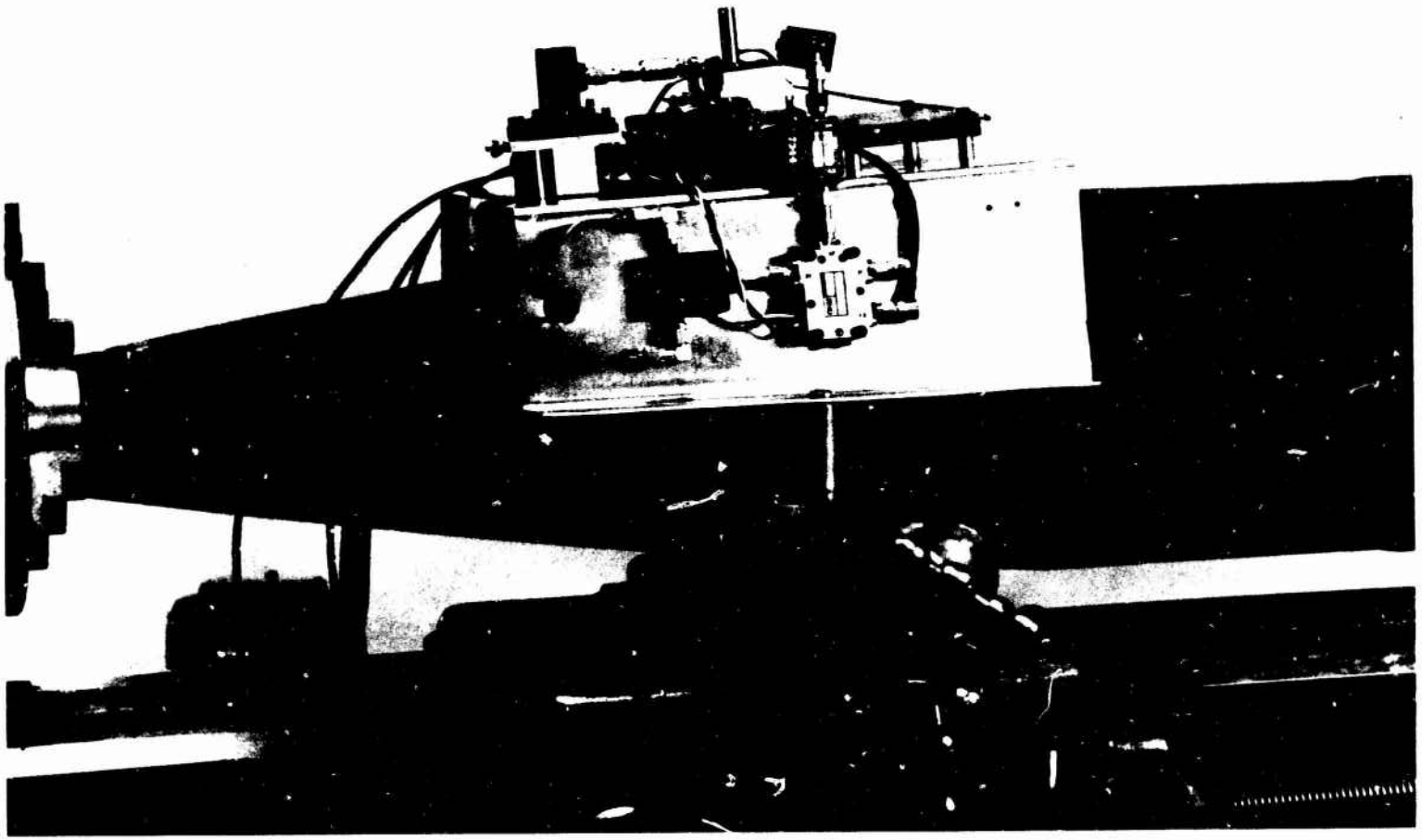

SA-2821 22

FIGURE 11 CURVED CRACK DETECTOR ON TESTED SHELL

as indicated in the block diagram of Figure 12. The functions and requirements of the individual ports of the low-frequency processing electronics are briefly explained. Following the quadrature IF mixer are two ac preamplifiers with 32 dB of gain, directly connected onto the mixer. These preamplifiers are designed for low noise figure and they reduce interference from other signals. The two channels are further amplified and filtered in active RC bandpass filters with a 3-dB bandwidth of 40 Hz (Q = 25). These bandpass filters pass only the fundamental frequency of the 1-kHz squarewave signal. Their main purpose is to reduce the receiver bandwidth in order to increase the sensitivity of the system. The bandpass filters are followed by precision halfwave rectifiers. Instead of a vectorial summation of the two channels representing quadrature components of the odd-mode signal, a direct summation is performed. This results in an error not exceeding 3 dB, which is tolerable if compared with other error-contributing factors in the system. Averaging of the sum-signal is performed with a low-pass filter. A logarithmic amplifier converts the output signal into a form far more desirable for observation and recording purposes. Finally, it was found useful to filter the logarithmic output signal in a high-pass filter with a cutoff frequency adjustable from 0.1 to 1 Hz. The operation of this filter performed on the logarithmic output signal can be looked at from two points of view. Firstly, the filter rejects low-frequency components of the output signal, which are mostly due to slowly varying changes in the spacing between the detector and the specimen. Secondly, the filter can be considered as an analog differentiator, yielding high impulses for rapidly changing output signals (crack-produced signals). Details about the operating mode of this high-pass filter will be presented in Section IV-B.

The low-frequency processing electronics were built by making extensive use of linear integrated circuits and RC active-filter design

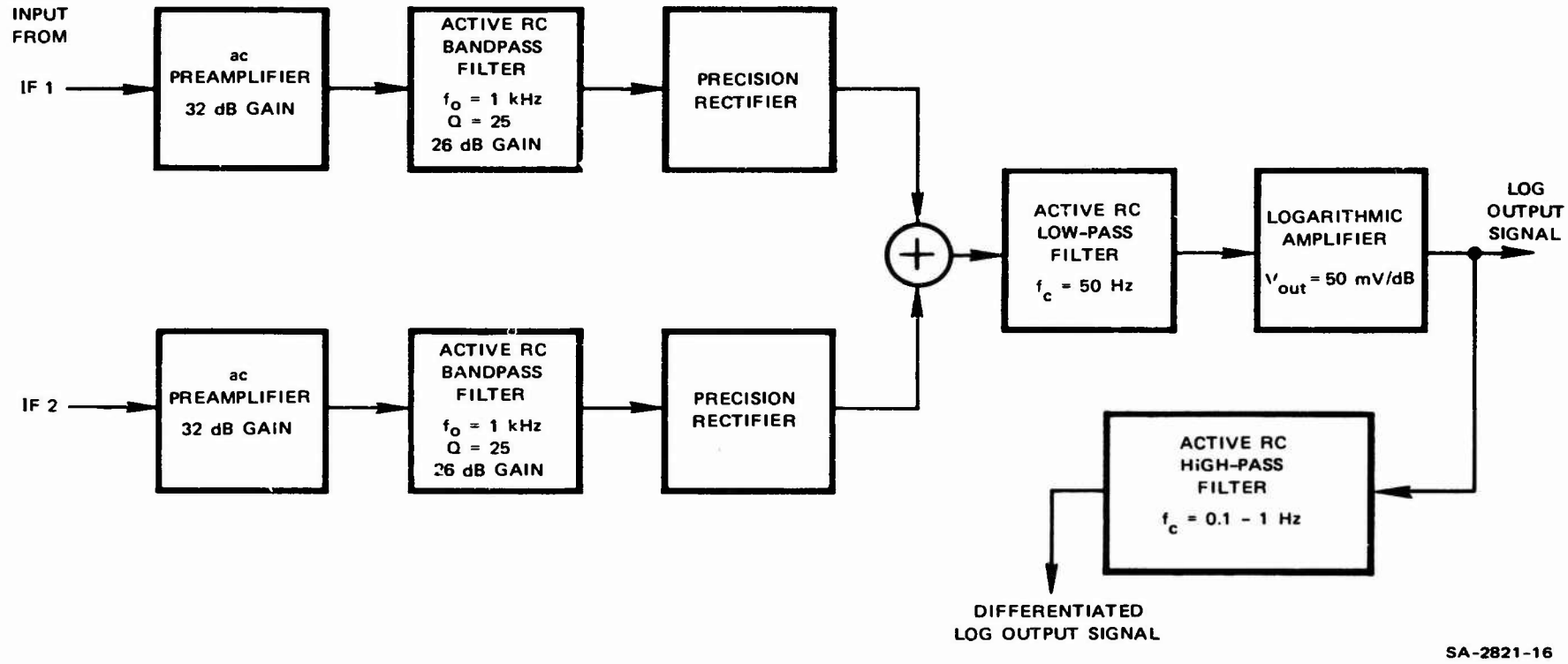

FIGURE 12 BLOCK DIAGRAM OF THE LOW-FREQUENCY PROCESSING ELECTRONICS

techniques. These techniques completely eliminate the need of bulky and expensive coils at audio frequencies. The complete circuit occupies a circuit board area of less than 5 by 6 inches. Figure 13 is a photograph of the complete crack-detector system with the curved detector on the left-hand side and the low-frequency electronic box on the right-hand side.

E. System Performance Tests

The important electrical parameter of the detector is the decoupling obtainable between the even- and odd-mode components at the difference output port of the rat-race hybrid. Typical measurement results for the curved detector are presented in Figure 14. They show the attenuation from the input port of the modulator to the sum and difference port of the rat-race hybrid. The difference between the two curves represents the decoupling that was obtained between the even and odd mode as observed at the difference port. For these measurements, the detector was placed on a shell without cracks and the system was tuned for maximum decoupling at 10.05 GHz. Any other frequency within the operating range of the oscillator, which is from 9.2 to 10.4 GHz, could have been selected for tuning to maximum decoupling. The attenuation of the sum signal of 25 dB is due to the losses of the various components between the switch and the rat-race hybrid. The cable and stripline losses, which amount to 15 dB in the measurements of Figure 14, are mostly caused by losses in the coupled stripline region. It was found later that the paint on the metal shell surface was primarily responsible for that loss. The maximum decoupling as observed in Figure 14 is 76 dB at 10.05 GHz. This is 18 dB less than calculated in Table 1. However, the measurement limit indicated in Figure 13 is not equal to the noise level of the receiver. Rather, this limit is determined by the precision rectifier (see Figure 12). Below a threshold level approximately 15 dB

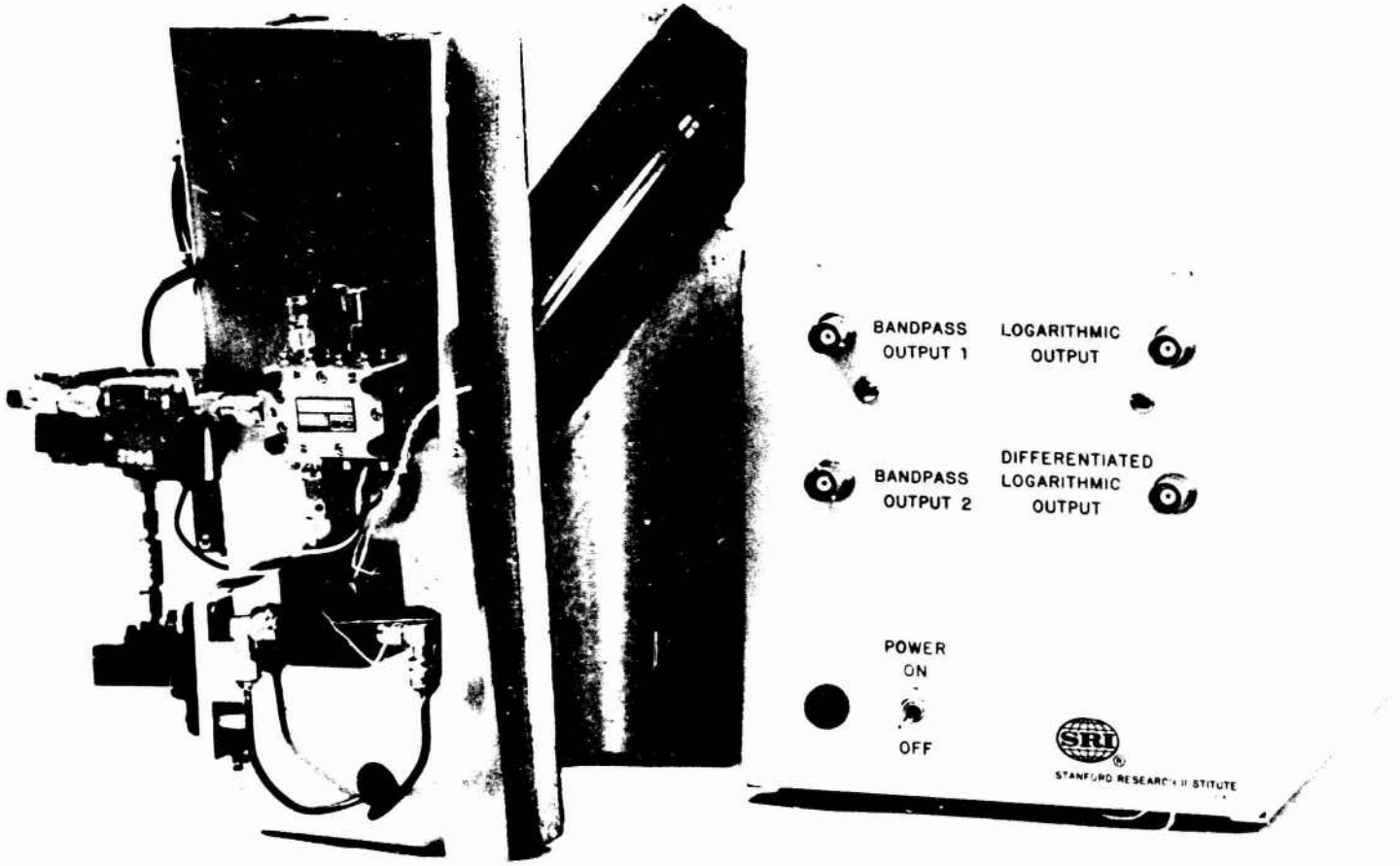

SA-2821-37

FIGURE 13 PHOTOGRAPH OF COMPLETE DETECTOR SYSTEM

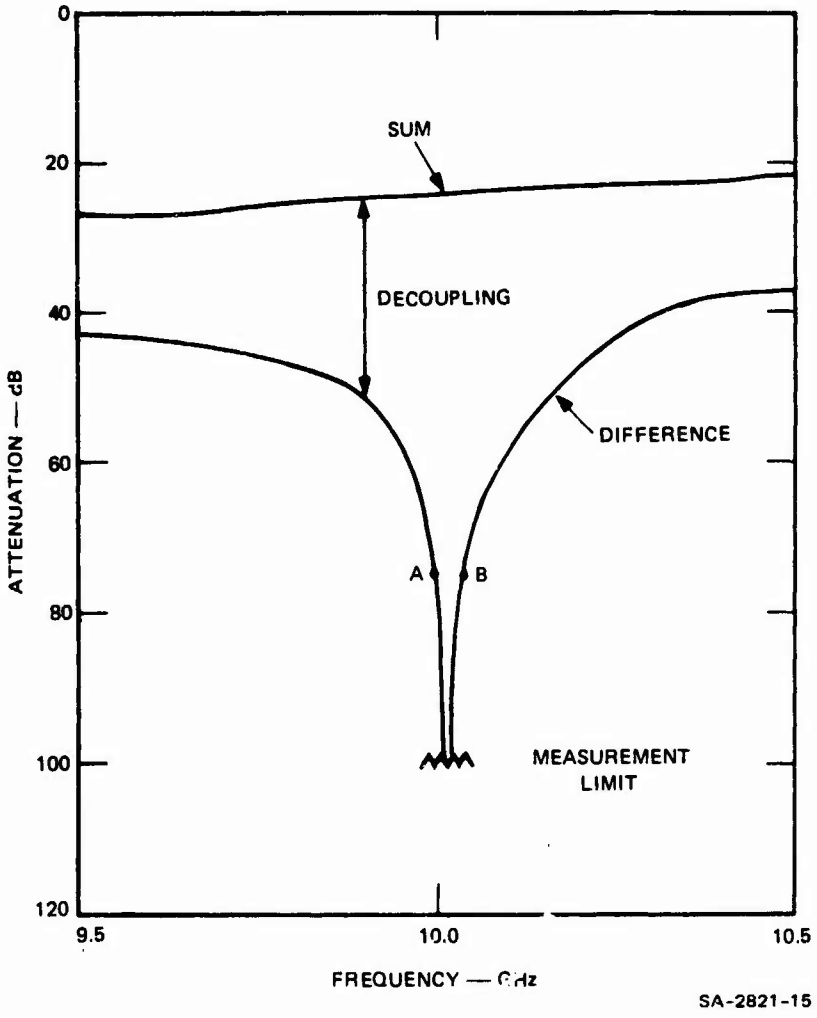

FIGURE 14 TRANSMISSION LOSS BETWEEN COMMON INPUT PORT (modulator input) AND SUM AND DIFFERENCE PORT OF THE RAT-RACE HYBRID FOR THE CURVED DETECTOR. The difference between the two curves represents the decoupling between the even mode and the odd mode.

above the noise level, the rectifier output remains constant. Taking this into account, the agreement between calculated and measured dynamic range is very good. The threshold effect of the rectifier has the additional advantage that it rejects the very noisy low end of the output signal, which would not be accurate and would only reduce the readibility of the output signal.

The true logarithmic characteristic of the overall low-frequency electronics was tested by injecting a 1000-Hz test signal into the active bandpass filter and observing the logarithmic output signal. In the range from 10 dB to 60 dB above the threshold level the deviations from a true logarithmic output are smaller than ±1 dB, and at the threshold level of the rectifier (measurement limit) they are 3 dB.

Tuning of the detector is quite easy. However, the decoupling rapidly drops to values around 50 dB once the detector is rotated around the shell (Points A or B in Figure 13). This effect is due to slight variations in spacing between the detector and the specimen. Its impact on the measurements will be further discussed in Section IV.

IV MEASUREMENT RESULTS

A. Measurements of Planar Plates

Initial measurements were done utilizing the planar detector (scanner) to test planar plates with machined cracks. Later, extensive measurements were made with the curved detector on the 175-mm artillery-shell bodies. The operating features of the planar and the curved detector were virtually the same. The initial measurements with the planar detector allowed us to test the completed detection system at an early stage of the project and to obtain signal samples for studying various signal-processing techniques. The planar detector proved very useful, and even though the main goal of the program was to build a detector for the artillery-shell bodies, some measurements on the planar plates are reported here. Some of the smallest cracks were measured with the planar detector because the surfaces of the test plates had a better finish than the shell bodies, which resulted in more ideal measuring conditions.

The planar scanner was mounted horizontally in a test fixture with the striplines pointing upward. Plates with various machined cracks were pulled at a constant speed across the scanner. The plates did glide on nylon screws that were adjusted for a flat travel. The output signal was recorded on an X-Y recorder, whose X-input came from the mechanical drive and was directly proportional to the travel length of the plates. Before any measurements were made, the crack detector was adjusted for maximum decoupling using a plain test plate of a plain section of a test plate with slots.

Preceding page blank

A total of seven plates with a large variety of machined cracks were measured. The crack dimensions varied within the following ranges:

Length	0.1 to 1.0 inch
Width	0.0015 to 0.031 inch
Depth	0.005 to 0.125 inch.

Most cracks had a constant depth, but some had the shape of a segment of a circle. The form of the cracks was straight linear, or sinusoidal, or trapezoidal. Also tested was a plate with bumps and ridges, which were fabricated mainly to study the effect of possible flaws of the test surface other than cracks. Figure 15 shows two test plates--Plate A with machined slots, and Plate B containing the bumps and ridges. The response for the Plate A with the slots depicted in Figure 15 is shown in Figure 16. The curve in the upper half of the graph represents the output signal or the decoupling in dB. The lower trace is the differentiated output signal. The abscissa represents either linear distance for the planar plates or angular position for the shells. Any artificial flaw is marked on the graph at the proper distance and with the correct physical extension and shape for easy comparison with the observed response of the detector. Each flaw, whether artificial or real, is labeled for ease of reference with a letter for the particular test object and a number for each flaw. The dimensions for the machined slots are also added to the graph. This type of representation remains the same throughout the report. However, the scales had to be changed on several graphs to accommodate the range of the output signals.

The graph of Figure 16 shows the response produced by five straight slots. Slots A1 through A3 were machined with a circular blade and therefore have the shape of a segment of a circle. Slots A4 and A5 have been cut with a small end-miller and are of a constant depth.

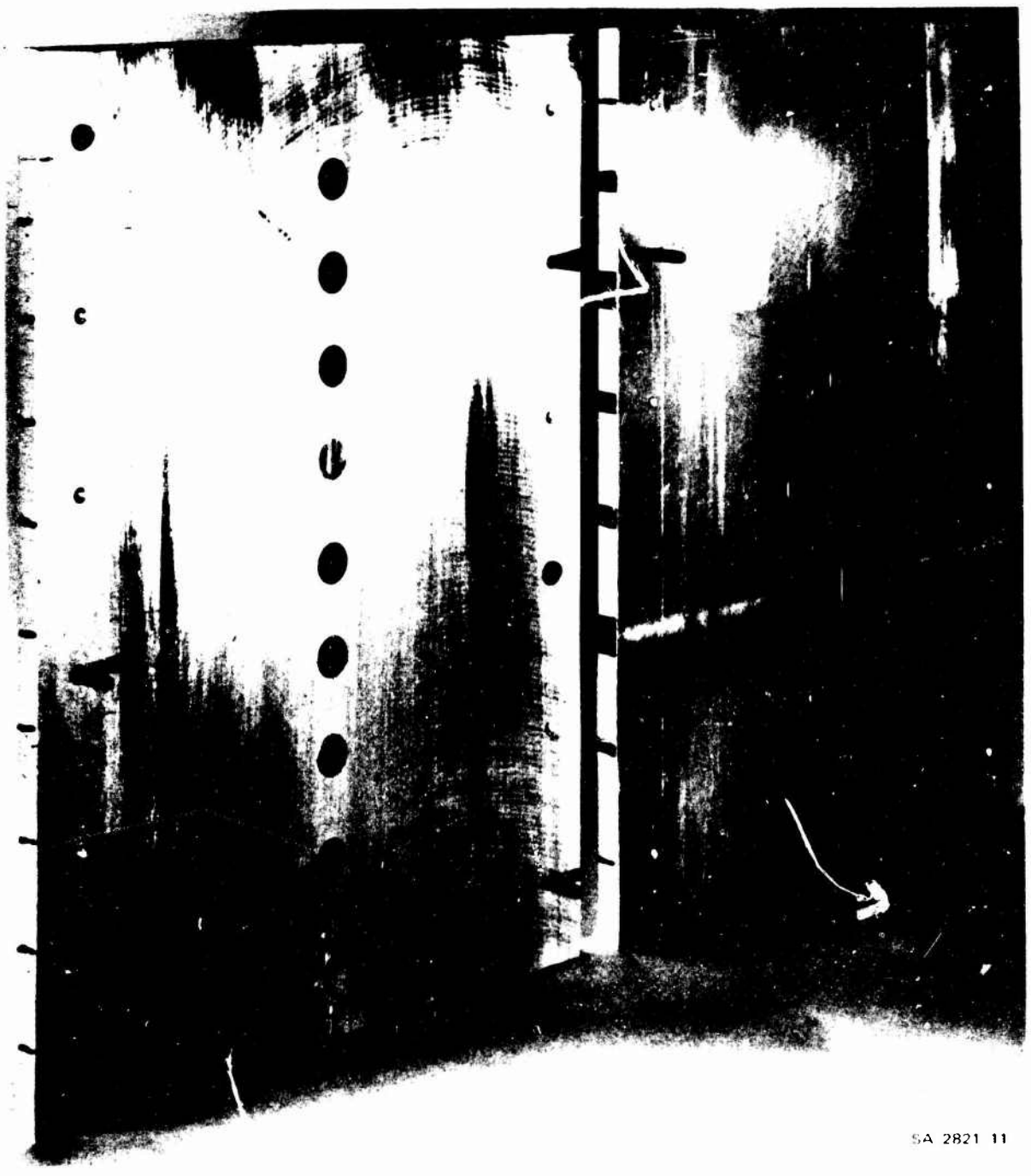

SA 2821 11

FIGURE 15 TEST PLATES WITH MACHINED CRACKS (right) AND BUMPS OR RIDGES (left)

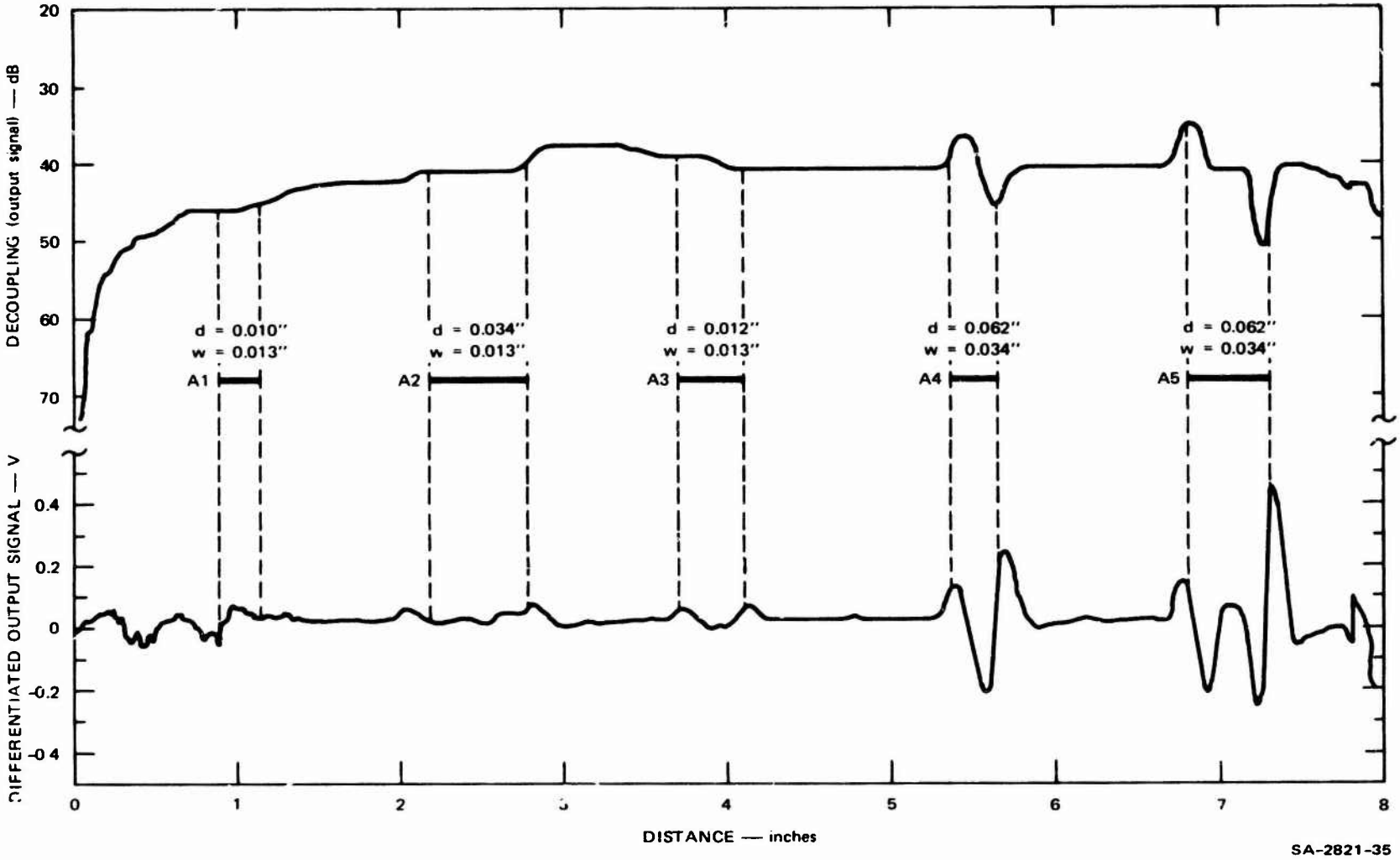

FIGURE 16 MEASUREMENT RESULTS FOR PLATE A WITH MACHINED SLOTS

Each crack is clearly discernible, particularly in the differentiated signal, where the beginning and end of each crack are marked by a pronounced pulse.

Figure 17 shows the results for the plate with bumps and ridges (see Figure 15, left side). The bumps as well as the ridges produce essentially the same response as cracks. Each perturbation is clearly visible. The results presented in Figure 18 represent the measurements on the smallest cracks performed so far. With a width of only 0.0015 inch and a depth of 0.005 inch, the one-inch-long crack C1 is still cearly discernible. But even with a length of only 0.1 inch (the width of one stripline) the crack would be visible.

B. Discussion of the Planar Measurements

After having presented the measurements on three different planar plates, we are in a position to discuss some of the characteristics that are common to the three measurements. In addition, we will be able to assess some of the features and limitations of the existing system in general. The following discussion will prepare the reader for the evaluation of shell-body measurements to be presented in Section IV-C.

Perhaps the most significant deviation of the present system from an ideal system is the fact that the output signal is not perfectly decoupled even without the presence of a crack. In all three measurements, the log output signal varies slowly over a range of 20 dB (Figure 18) to more than 30 dB (Figures 16 and 17), if the crack-produced deviations are neglected. This slowly varying component is generated by small variations in the spacing between the detector and the test object, and we shall refer to it as the background signal. This signal has important implications for the detectability of cracks and also for the

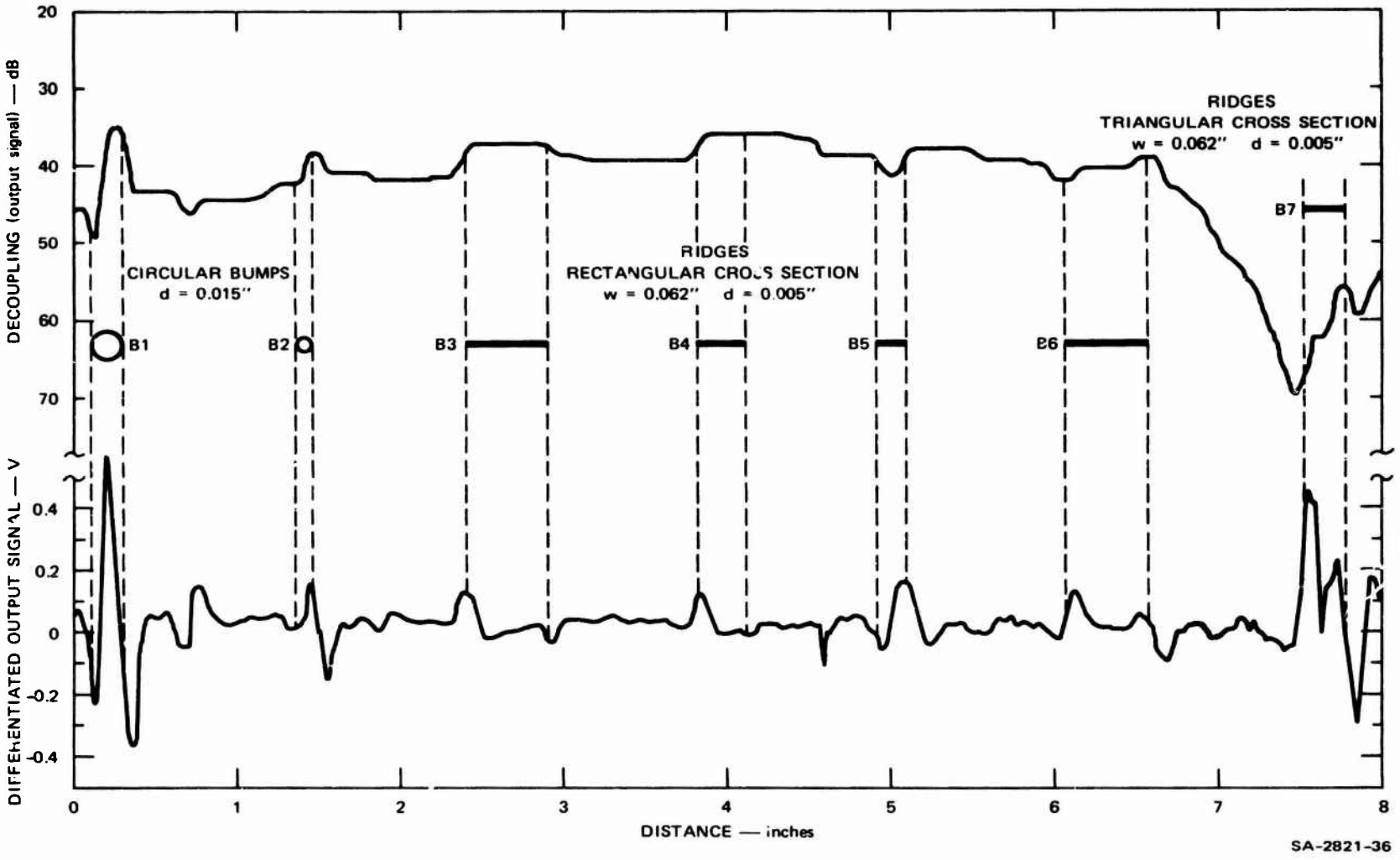

FIGURE 17 MEASUREMENT RESULTS FOR PLATE B WITH BUMPS AND RIDGES

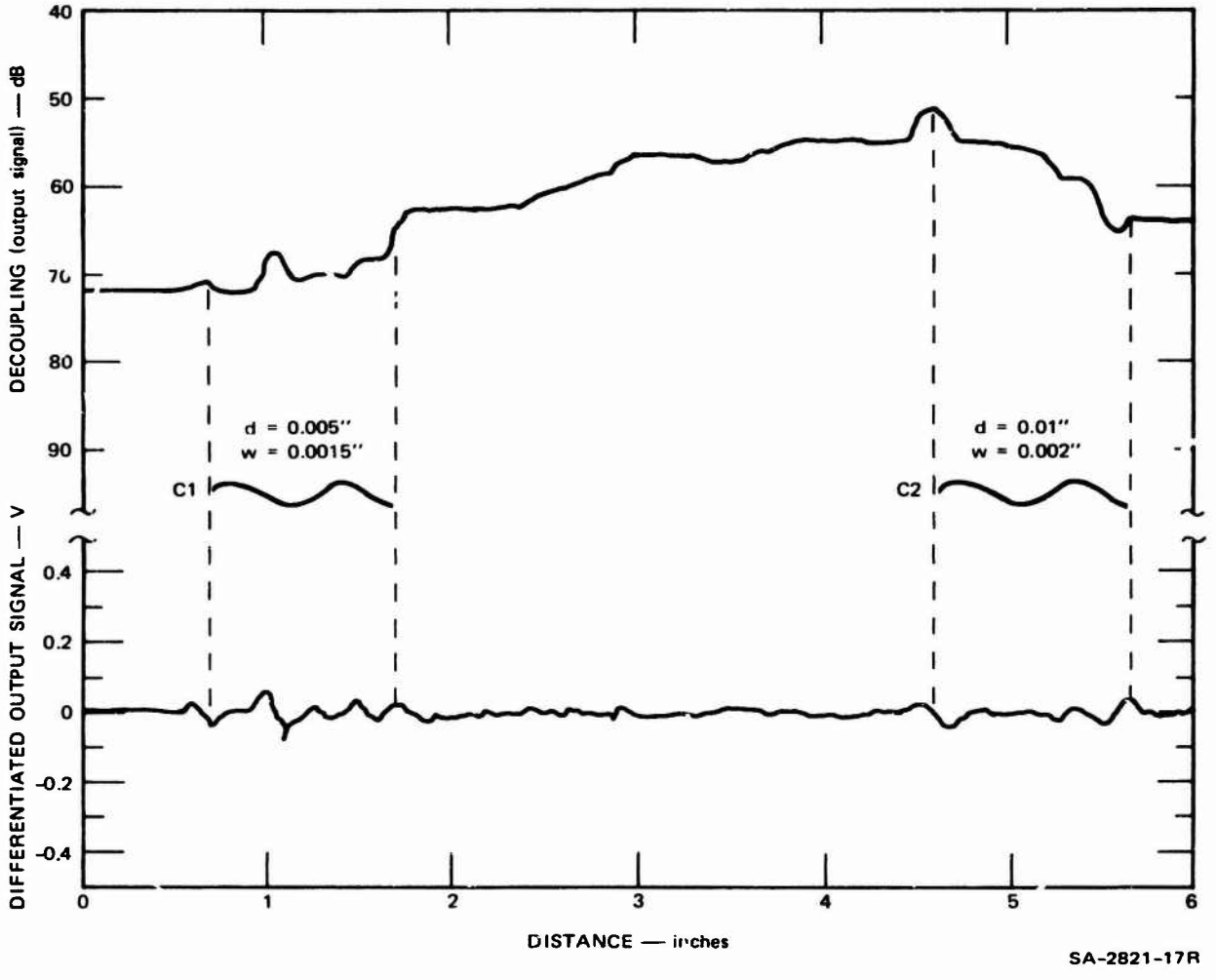

FIGURE 18 MEASUREMENT RESULTS FOR PLATE C WITH TWO WIGGLY CRACKS

typical waveforms that will be produced during scanning of a crack. Filtering of the output signal with a high-pass filter is, of course, the simplest signal processing that can be done to eliminate the slowly varying background signal and to emphasize the crack-produced signals.

The analysis of the theoretical output signal for a point perturbation and a finite perturbation, as presented in Section II-D, is correct only for the case of a perfectly decoupled system. A system retaining the phase information would yield the waveform shown in Figure 4(b). However, because our system indicates only the amplitude information, the result is a waveform as shown in Figure 19(a), Waveform (1). For a

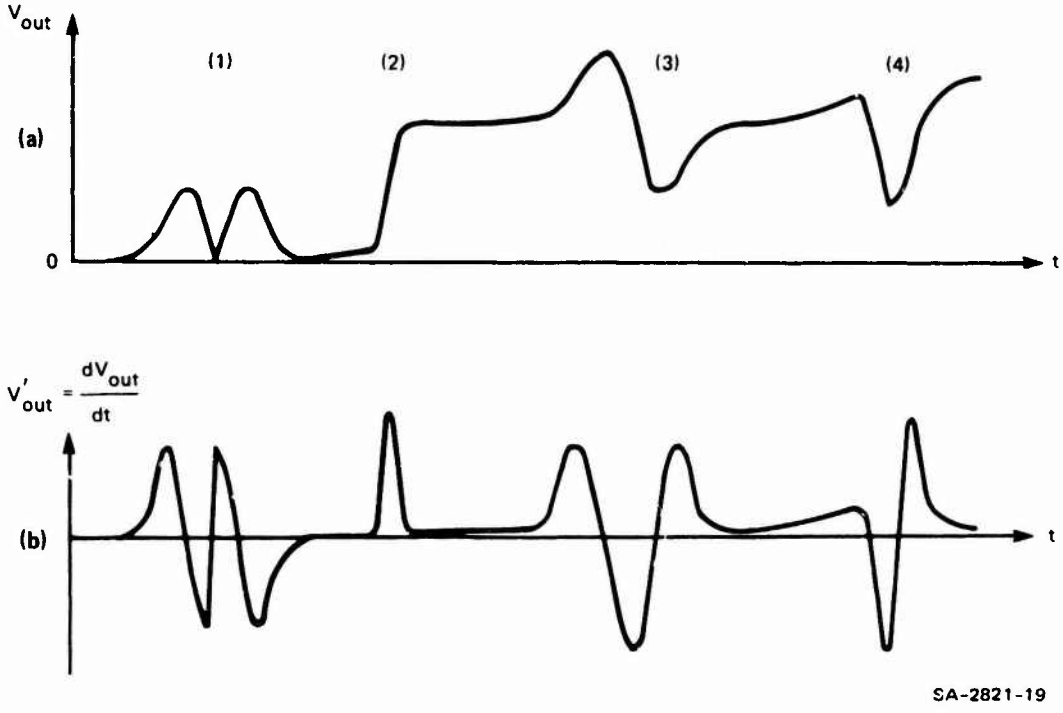

FIGURE 19 TYPICAL CRACK-DETECTOR OUTPUT WAVEFORMS

background signal that is not negligible, the situation is different. The phasors for the output signal for this case are illustrated in Figure 20. The output signal, V_{out}, is the vector sum of the crack-

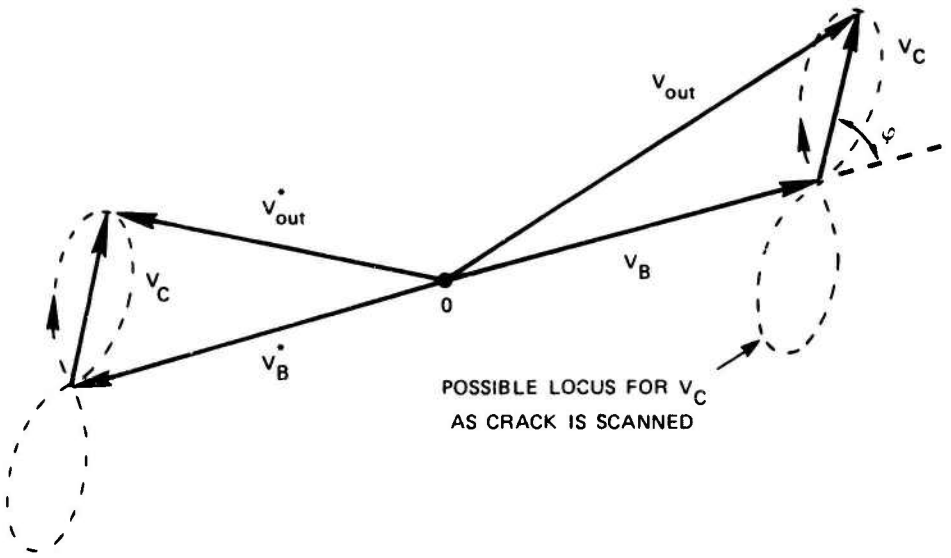

SA-2821-20

FIGURE 20 CRACK-PRODUCED OUTPUT SIGNAL UNDER THE CONDITION OF A LARGE BACKGROUND SIGNAL

produced signal, V_C, and the background signal, V_B. As the detector scans a small crack, V_C changes in amplitude and phase, probably following a locus indicated by the dashed curve. For $V_B = 0$, $|V_{out}|$ will be exactly as shown in Figure 19(a), Waveform (1). However, for $V_B \neq 0$, $|V_{out}|$ will be more like a single sine wave superimposed on a constant value that is equal to $|V_B|$ [see Figure 19(a), Waveform (3)]. The response for Crack A4 in Figure 16 is clearly of this type.

Two important conclusions can be drawn from the above analysis:

(1) If the signal V_C is perpendicular to V_B, almost no change in V_{out} will occur, unless $|V_C|$ becomes comparable to or larger than $|V_B|$. Because no control is available over the phase relationship between V_B and V_C, this situation can be remedied only by minimizing V_B.

(2) Let us assume that the signal V_B corresponds to operating at a frequency below that of maximum decoupling, f_0--e.g., Point A in Figure 14. Changing the frequency to a point above f_0 (i.e., Point B) will reverse the sign of V_B

as indicated in Figure 20 by V_B^*. However, the small frequency change involved does not change V_C. The result is that the output signal for the same test object measured at frequency points symmetrical about f_0 should be complementary to each other. This was verified experimentally with high accuracy.

For cracks of a more general shape (e.g., wiggly or circular shape), the output signal will no longer have the characteristic Waveforms (1) or (3) as indicated in Figure 19(a). The only characteristics common to all localized disturbances is that V_B will remain relatively constant while the disturbance is being scanned. Therefore, the simplest waveform that can be due to a crack is a single pulse in V_{out} as illustrated by Waveform (4) of Figure 19(a). On the other hand, measurements on wiggly-shaped cracks result in a long series of pulses. However, a single step in V_{out}, as indicated by Waveform (2) in Figure 10(a), can be attributed only to a change in the background signal V_B. Such changes are most likely the result of sudden changes in the spacing between the detector and the test object.

As mentioned above, high-pass filtering (or differentiating) of the output signal results in the rejection of lowest-frequency components that cannot be due to any cracks. The effect of differentiating the sample signal of Figure 19(a) is shown in Figure 19(b). The new signal, V'_{out}, indicates a simple way of discriminating between cracks and abrupt changes in the spacing that are not eliminated by the high-pass filter. The abrupt changes result in a single pulse for V'_{out}, whereas cracks must result in at least a sequence of two pulses of opposite polarity in V'_{out}. Based on this characteristic, a simple detection logic could be constructed that could discriminate between cracks and abrupt changes in the spacing between the detector and the specimen. Details of such a method will be discussed in Section V-B.

It should be clear that the high-pass filter only approximates the differentiating process for the output signal, because frequencies higher than the cutoff frequency of the filter are passed undistorted. It was found that best results are obtained if the cutoff frequency of the filter is chosen as the inverse of the time that is required to scan a distance equal to the total width of coupled striplines, $2w + s$. In the present setup, this time was 1 s and the filter cutoff frequency was 1 Hz.

Though it seems that the high-pass filter eliminated any problems associated with the background signal, two severe effects remain. The first effect was mentioned above and has to do with the possible orthogonality of the crack-produced signal and the background signal, and with the almost complete loss of sensitivity for such cases. The one solution to this problem is a reduction of the background signal to levels smaller than the crack-produced signal from the smallest anticipated crack. The second effect is closely related to the first one. In order to obtain a crack-produced change of 3 dB on top of a given background signal, the former signal has to be 40% of the amplitude of the background signal. Therefore, if a signal change of 3 dB is considered the minimum that can be detected, the sensitivity over most of the scan in Figure 16 is only around 43 dB and not 75 dB or better as determined from system performance tests. In addition, as the background signal varies, so does the sensitivity. This is, of course, unacceptable for quantitative measurements. However, this is not an insurmountable problem, and a suggested solution to it will be presented in Section VI-A.

It seems appropriate at this point to try to compare the measured coupling of a given crack with the computed value from Section II-C. For this test, we take the crack number A4 of Figure 16. There the crack produced a signal that deviated 4.5 dB from the background signal

that was 40 dB down from the even-mode level. Assuming that the two signals were in phase, we determine for the crack a coupling factor of -43 dB. Based on the analysis of Section II-C, we calculate for the same crack a theoretical coupling factor of -32 dB.* The agreement for this case is poor. It is possible that V_C and V_B are not in phase with each other, which reduces the response somewhat. However, it is more likely that the calculations are not accurate enough, because the size of the crack is too large for the simplifying approximations that were made. A similar comparison for the smallest crack measured, number C1 of Figure 18, yields a measured coupling factor of -84 dB compared with a calculated value of -80 dB, which is in much better agreement than in the previous case. This indicates that the simplified model used for the calculations breaks down for a crack as large as A4.

C. Measurements on the Artillery-Shell Bodies

In all of four available shell bodies, artificial cracks were produced. In the first shell, we machined holes of 0.40 inch diameter. Then plugs with slots were inserted and the curved surface of the shell was carefully restored. A total of four plugs were distributed over the active area of the detector and spaced in a way that made them appear about equally distributed over a full circumferential scan, when tested with the curved detector. The slots that were produced in this way had

---

*For long cracks, the length that has to be entered in Eq. (8) is no longer that of the crack itself, but is the width of one stripline, or 0.100 inch. This width is a good approximation to the width that would contain the same total current in the test surface at the peak current density as the total current flowing in one-half of the total test surface (one-half of the x-axis). The reason for this measure is the fact that a long crack produces the maximum output signal when the crack intercepts all currents in one-half of the test surface.

a constant depth of 0.125 inch, a length of 0.50 inch, and a width of 0.006 inch or 0.010 inch. The angles between the cracks and the axis of the shell, θ, were selected to be 0°, 45°, and 90°. Figure 21 shows the shell with two of the four plugs visible. The measurement results for that shell are given in Figure 22. Again, the upper trace represents the logarithmic output signal and the lower trace is the derivative of the upper trace. All four cracks are clearly discernible. However, three more areas with marked impulses in the lower trace can be observed; they are labeled D5 through D7. Originally, we believed that these strong responses are the result of real cracks. Later, it turned out that their origin lies in the plugs themselves. The shells came originally with a protective paint. This paint can be considered as a lossy dielectric and has a significant influence on the transmission characteristics of the striplines. The plug itself has no paint, and on the surface surrounding the plug the paint was partly removed because of the surface refinishing after the plug was mounted. Therefore, the responses D5 through D7 are the result of the missing paint and/or of a slight deviation of the surface of the shell from its proper shape in the vicinity of the plugs. The average decoupling in the measurement of Figure 22 is only 50 dB, and therefore the sensitivity is not better than 53 dB.

In order to learn more about the effect of the plugs themselves and the effect of the paint, we prepared a second shell with two empty plugs. One plug was tightly fitted, as were the plugs on the previous shell. A second plug had a clearance of 0.001 inch extending 0.125 inch deep from the surface into the shell body. Figure 23 shows the measurements for that shell. Both plugs produce large responses. The tightly fitted plug generates a narrow pulse in the output signal, mainly because the surface of the shell had not been restored perfectly. The plug with the 0.001-inch tolerance exhibits the same kind of response,

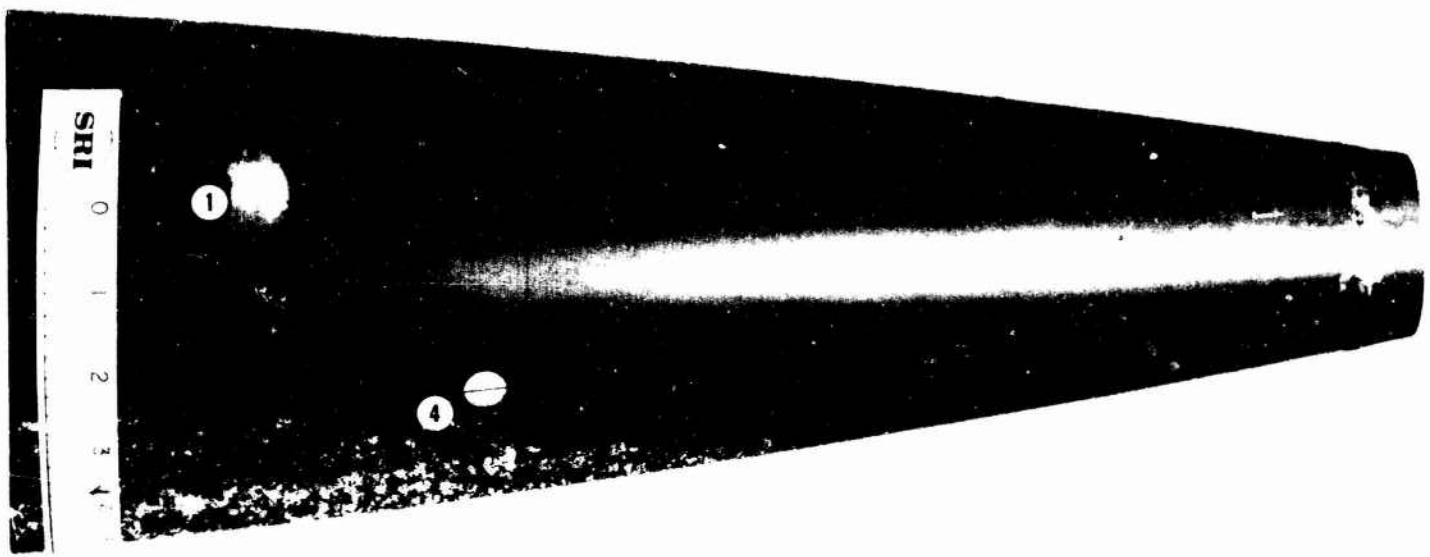

SA 2821 21

FIGURE 21 SHELL D WITH "PLUG-TYPE" CRACKS

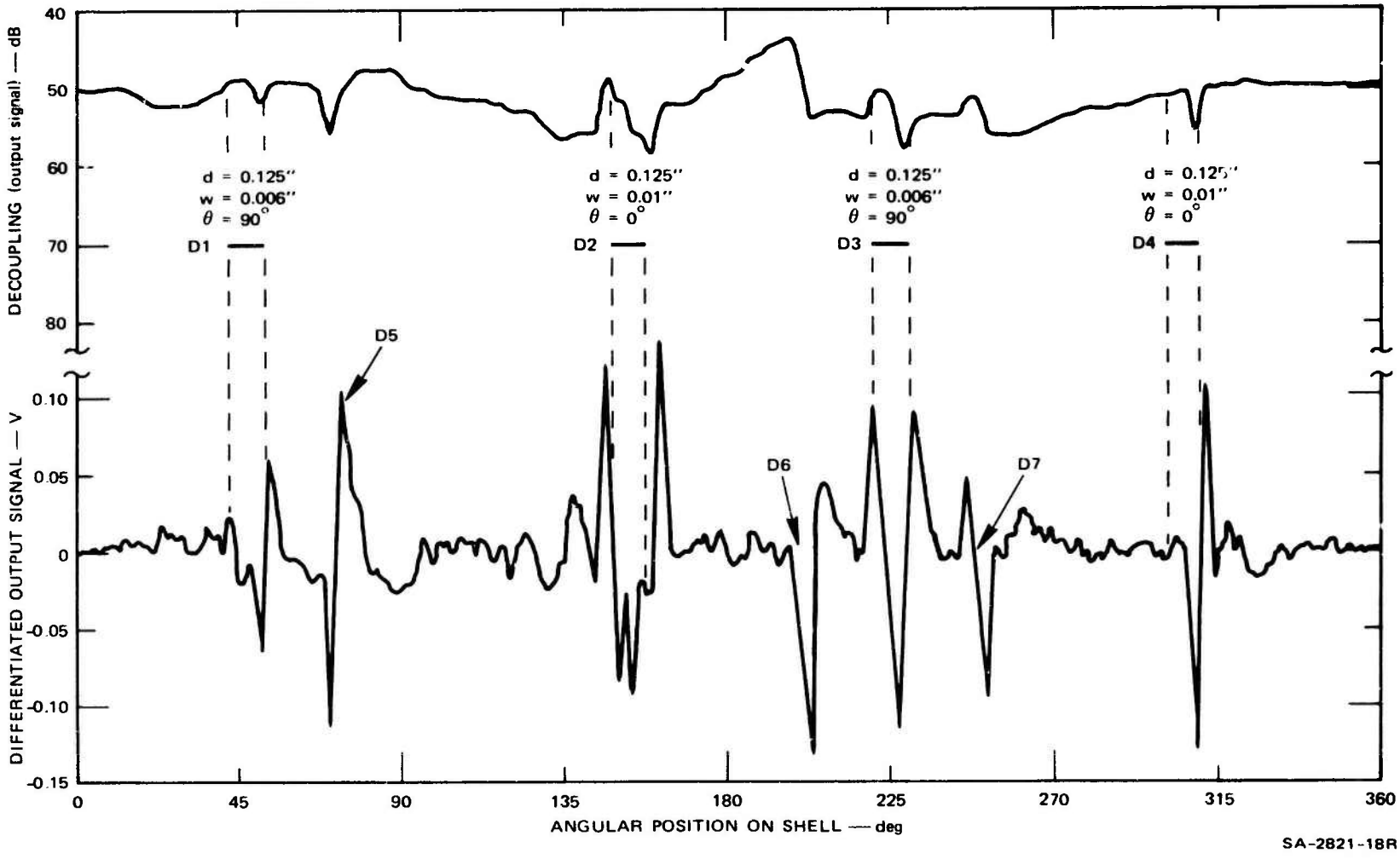

FIGURE 22 MEASUREMENT RESULTS FOR SHELL D WITH "PLUG-TYPE" CRACKS

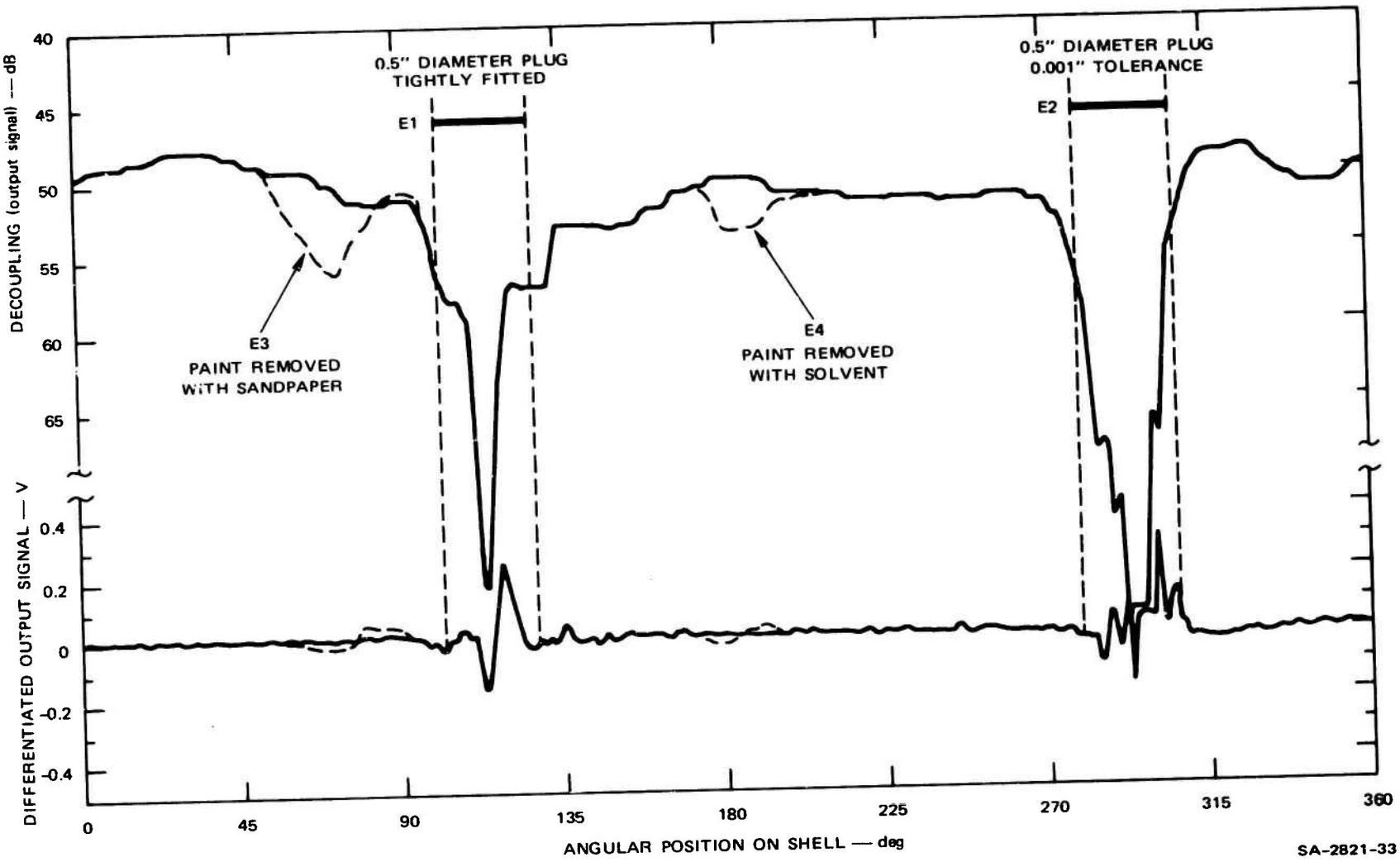

FIGURE 23 MEASUREMENT RESULTS FOR SHELL E WITH EMPTY PLUGS

though wider, which clearly shows the effect of the 1-mil gap. In order to better identify the cause of the strong responses for the empty plugs, we removed the paint at two places without removing and retuning the detector. The response labeled E3 was created by removing the paint in a 0.75 inch-diameter area with sandpaper. Likewise, the deviation E4 occurred after the paint was removed in a 0.5-inch-diameter area with a solvent. It is not known at this time whether it is the losses or the dielectric effect of the paint that is more significant in generating the response observed. Either of the two effects creates an imbalance that is detected by the stripline crack detector. As a conclusion, we can state that the results for the "plug-type" cracks of Shell D have to be interpreted very carefully. Cracks numbered D2 and D3 clearly show the typical response for a crack, with D1 not quite as clear. But the response for D4 is not unequivocally identifiable as that of a crack.

The third shell yields better results in that the surface of the shell was not disturbed around the machined cracks. Those were cut with a 1-inch-diameter circular saw blade and therefore the slots have the shape of a segment of a circle. The cracks have a maximum depth of 0.1 inch, a length of 0.8 inch, and widths ranging from 0.006 inch to 0.01 inch. The angles between the cracks and the axis of the shell, θ, were again selected to be 0°, 45°, and 90°. The response for this shell is given in Figure 24. All cracks are detected easily by the stripline detector.

Finally, very small slots were fabricated by electro-discharge machining. By this technique, we were able to get slots of a constant depth of 0.01 inch and 0.02 inch and not wider than 0.0035 inch. The length of these cracks is 0.25 inch or 0.50 inch.

Machining of these cracks required removal of the paint in the area of the crack. Therefore, valid measurements were possible only after

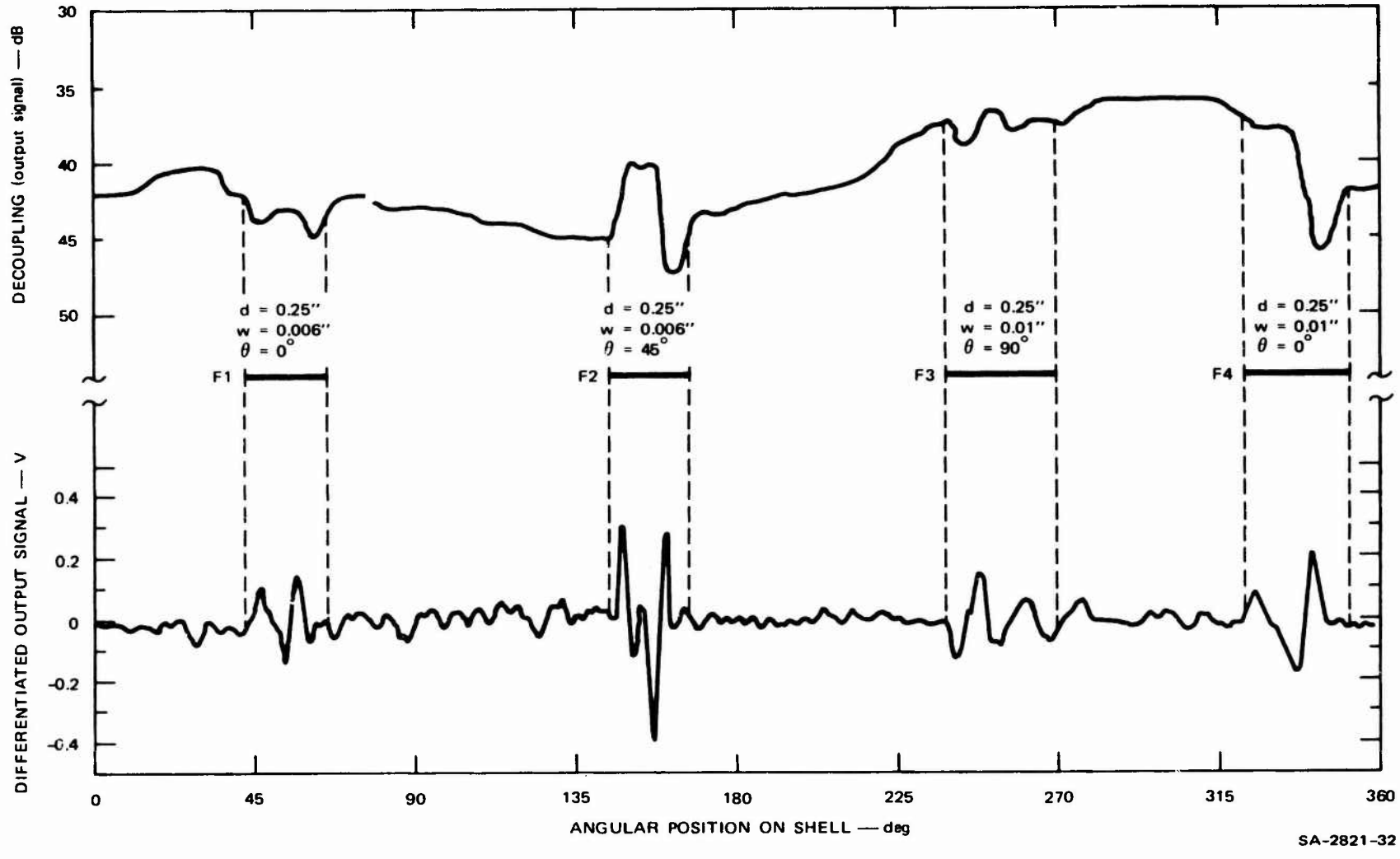

FIGURE 24 MEASUREMENT RESULTS FOR SHELL F WITH SAW-BLADE-CUT CRACKS

the paint had been removed in the whole area that is scanned by the detector. The small cracks in Shell G required that the system be tuned to a high average decoupling. After some trial runs, we found a tuning condition with better than 60 dB over the full scan. The result for this run is shown in Figure 25. All four cracks yield fluctuations of the differentiated signal that are larger than the fluctuations in "quiet" areas. However, many more flaws are detected. Three of them, G5 through G7, have been positively identified as small abrasions on the shell, roughly 0.5 inch long and 0.1 inch wide. They are probably caused by the mounting fixture for the shell that was utilized while machining the cracks. We have not been able to identify positively any other pulses with a flaw on the shells. However, a brief quantitative calculation will show that very minor changes in the surface are sufficient to generate a pulse of a magnitude similar to or larger than that of a crack. The active volume of the smaller cracks on Shell G is $0.01 \times 0.0035 \times 0.1 = 3.5 \times 10^{-6}$ inch^3. Now let us assume that we have a localized area on the shell that is 0.001 inch deeper than the surrounding surface. An area not larger than 0.1×0.035 inch is sufficient to give the same volume as the smallest cracks and therefore also the same response. This example should make it clear that the smallest surface unevenness quickly generates an output signal comparable to that of the smallest cracks. This problem is inherent in the stripline crack detector. Anything that unbalances the even mode on the striplines produces an output signal irrespective of the nature of that asymmetry.

D. Final Discussion of the Measurements

The measurements presented in this report are representative of many more that were made during the course of the project. The measurements performed on the shell bodies did not reveal any basic characteristics

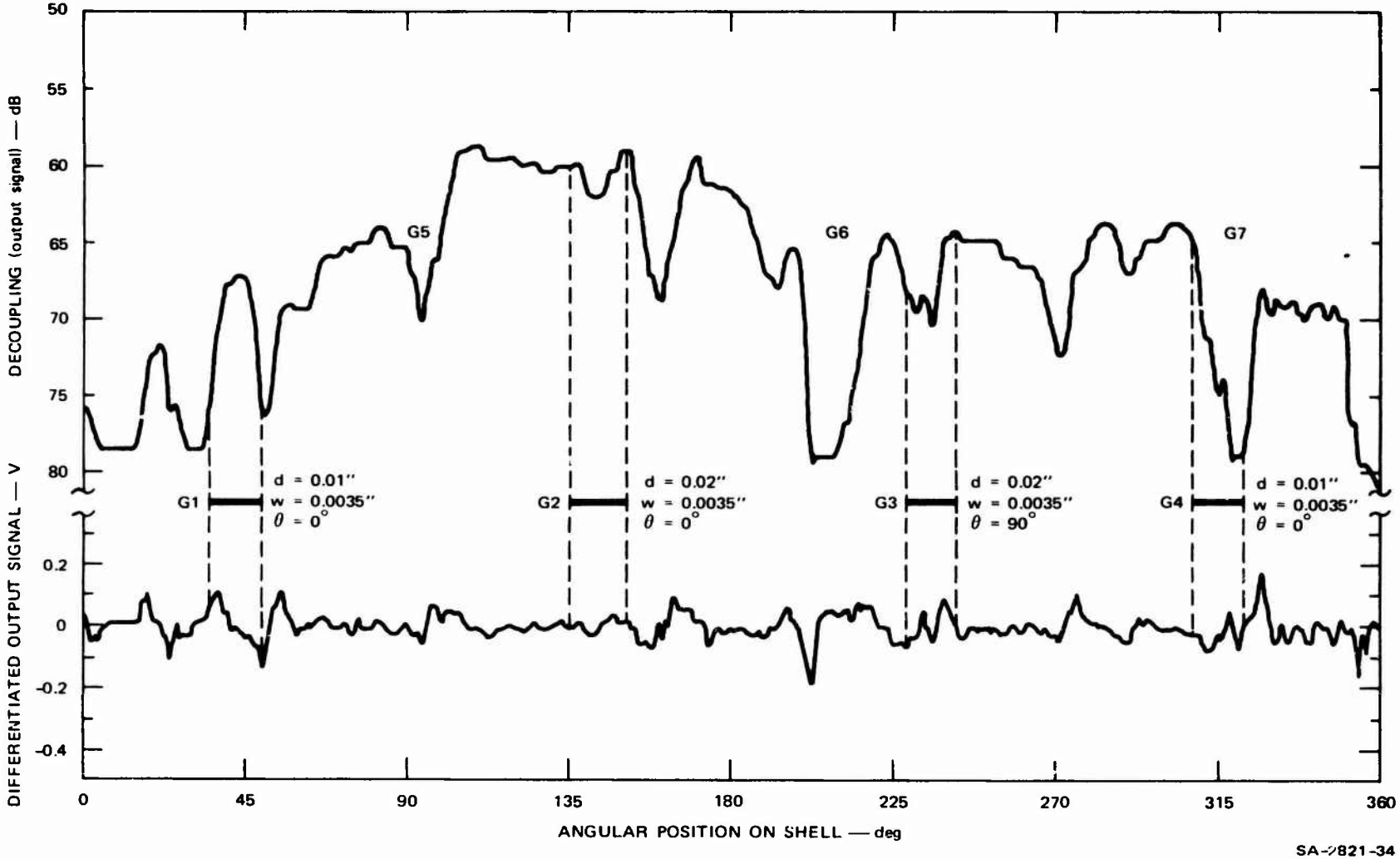

FIGURE 25 MEASUREMENT RESULTS FOR SHELL G WITH ELECTRO-DISCHARGE-MACHINED CRACKS

of the stripline crack detector that are different from those already known from the planar setup. Minor differences involve the effect of the paint of the shells and the difficulty encountered with the plugs. The basic characteristics of the system are summarized below.

Background signals as large as only 40 dB down from the even-mode level are unavoidable in the present system. The effect of these signals on the system is a reduction and variation in sensitivity and the possible loss of detection, even for large cracks, as explained in Section IV-B. To reduce the sensitivity variations, the detector was sometimes purposely detuned to a decoupling of 50 dB (see Figure 23) corresponding to Point A or Point B in Figure 14. This was done at the price of reduced sensitivity. Though all machined cracks have been detected with the present system, cracks of equal size sometimes produced responses of different amplitude (see, for example, D1 and D2 in Figure 22) which is believed to be the result of different phase angles between the crack-produced signal and the background signal as illustrated in Figure 20. The only solution to both problems is a low and constant background signal.

Intuitively, it seems possible to derive a compensation signal for the background signal in a different way--e.g., by measuring the average spacing between the detector and the test object. In theory, a perfectly symmetrical detector (with respect to a plane perpendicular to the stripline surface and parallel to the coupled striplines) should have a decoupling of the odd-mode from the even-mode signal that is independent of variations in spacing between scanner and test object. However, the background signal is the vector sum of many contributions to the odd-mode signal from localized asymmetries in the spacing. Therefore, any attempt to measure the average spacing for compensation purposes, be it mechanically or electrically, must fail. There exists no method by which the background signal can be obtained other than by the original

process itself. A different approach using a feedback system to vary the RF frequency and thereby maintain optimum decoupling as spacing varied was studied toward the end of the contract and led to some promising results. Details of that solution will be presented in Section VI-A.

The characteristic crack-produced signal derived in Section II-D and shown in Figure 19(a), Waveform (1), was never observed. We found that a localized flaw produces at least a sequence of two pulses in the differentiated signal that have opposite signs and are closely spaced (e.g., see E1 in Figure 23). The magnitude of these pulses reflects the size of a crack, but quantitative measurements are not possible with the present system because of the varying sensitivity. On the other hand, a pure and abrupt change in the spacing between the detector and the test object yields only a single pulse in the differentiated output signal. Other than this, very little can be predicted concerning the nature of the waveforms for a crack. Occasionally almost perfect responses are obtained, as is the case for D3 in Figure 22, which are exactly the predicted waveforms (3) in Figure 19(a) and (b). The lack of any typical waveform is of great significance for the type of signal processing that can be performed on the measured output signals. Details of the various signal-processing techniques investigated are presented in the next section.

V SIGNAL PROCESSING

A. Theory

The function of the signal-processing part of this project was to develop or adapt techniques that would provide means of recognizing the existence of a crack from the output signals of the crack detector. The output signal is in the form of a continuous trace of voltage versus time, and the function of the processing technique is to detect the desired part of the signal and the desired information unambiguously and with minimum time delay.

The first approach to the problem of recognition of cracks was based on use of correlation techniques and spectral analysis.* A characteristic signal of a crack--its signature--was to be used as the basis for identification of other cracks interacting with the surface-scanning system.

In correlation procedures, two signals are compared with each other and their commonality is indicated by the value of the correlation function of the two signals:

$$\Psi_{xy}(\tau) = \frac{1}{2T} \int_{-T}^{T} x(t)\, y(t - \tau)dt \qquad (12)$$

---

*For a thorough review of correlation techniques, see the book by Lange.[8]

where

$2T$ = Time period of scan of signals

$x(t)$, $y(t)$ = Two signals being compared

τ = Displacement in time of one signal with respect to another.

If $x(t)$ is the same signal or waveform as $y(t)$, the correlation then becomes

$$\Psi_{xx}(\tau) = \frac{1}{2T} \int_{-T}^{T} x(t)\, x(t - \tau) dt \quad , \tag{13}$$

the autocorrelation. This function is symmetrical about the value $\tau = 0$, and $\Psi_{xx}(0)$ is the mean square value of the function.

As the difference between $x(t)$ and $y(t)$ becomes greater the value of the cross-correlation function (12) decreases. This decrease is an indication of the discrepancy between the two signals under comparison. The cross-correlation function can also be considered as the mean value of the product of the two signals--i.e., $x(t)\, y(t - \tau)$.

This concept of mean values leads to consideration of using the cross-correlation factor as an indication of similarity between the reference signal and the signal from the surface scan. This factor may be written as

$$\gamma_{xy}(\tau) = \frac{\Psi_{xy}}{x_{rms} y_{rms}} \leq 1 \quad . \tag{14}$$

where x_{rms} and y_{rms} are the root-mean-square values of x and y over the period 2T, respectively. If the two signals are the same, the ratio is one and it decreases as the similarity decreases.

By taking the Fourier transforms of the auto- and cross-correlation functions, one gets the power density spectrum or spectral density

$$S_{xx}(f) = \int_{-\infty}^{\infty} \Psi_{xx}(\tau) e^{-j\omega\tau} d\tau \qquad (15)$$

and the cross spectrum

$$S_{xy}(f) = \int_{-\infty}^{\infty} \Psi_{xy}(\tau) e^{-j\omega\tau} d\tau \qquad (16)$$

where $\omega = 2\pi f$. The expression for spectral density is commonly called the auto-spectrum and it represents the average spectral power in the signal or waveform under study. Analogously, the cross-spectral function represents the degree of common frequency components of the two signals being compared. A ratio describing the correlation between the two signals in terms of frequency is the coherency spectrum:

$$K_{xy}(f) = \frac{S_{xy}(f)}{[S_{xx}(f) \cdot S_{yy}(f)]^{\frac{1}{2}}} \quad . \qquad (17)$$

Applied to the present detector system, correlation techniques seemed ideal to recognize cracks in the output signal. All that has to be done is to correlate the known response of a crack as given by s(x) in Figure 4(a) with the output signal. One can calculate either the cross-correlation function (12) or the cross-spectrum. Whenever a portion of the output signal is similar to the charcteristic crack-produced signal,

the cross-correlation function will exhibit a large value or the cross-spectrum will exhibit large spectral lines. In the present system, all signals are measured and recorded as functions of time. However, they are actually functions of distance or angle and any spectral transforms like the Fourier transform or the cross-spectrum do not represent spectral content in the frequency domain; rather, they represent harmonics in space. To be more specific, when the planar scanner moves across the specimen at a constant velocity, its output signal can be considered as a function of χ, the displacement of the perturbation from an origin $\chi = 0$. The signal is $f(\chi)$ rather that $f(t)$. The Fourier transform of this signal then becomes $F(\lambda)$ rather than $F(\omega)$, where λ can be considered as $2\pi n/L$ (L is specimen length) and is an indication of oscillations per unit length rather than per unit time. However, the concepts associated with spectral density still apply.

As is known from the experimental work, it was impossible to find a characteristic crack-produced signal that uniquely identified a crack. Rather, many different waveforms were found, all generated by simply formed cracks. In practice, the variation in possible waveforms would be even greater because real cracks would have random shapes. This indicates the difficulty we encountered when we tried to apply correlation techniques to recognize cracks. Some practical results will be presented in Section V-B.

B. Signal-Processing Experiments

All measurements performed on plates and the shells were recorded on a Honeywell instrumentation tape recorder. These recordings were later analyzed by means of a Time Data time-series analyzer. The operations performed include Fourier transform, the power spectrum, the autocorrelation function, the cross-correlation function, and the cross-spectrum.

In order to perform these operations, the analog input signal was sampled and digitalized. Then a digital computer performed the various operations, which are all based on the fast Fourier transform. Our analyzer operates on frames of 1001 samples. The sampling rate is adjustable from microseconds to milliseconds. This, in turn, determines the period, T, of the sampled signals.

As pointed out previously, the scanning motion produces the output signal $V_{out}(t)$, where t represents time. However, the signal is more meaningfully interpreted as $V_{out}(\chi)$ or as $V_{out}(\varphi)$, where χ is the linear displacement of the planar scanner and φ is the angular displacement of the curved detector. $V_{out}(\chi)$ or $V_{out}(\varphi)$ have the advantage of being independent of the scanning velocity.* However, for the sake of simplicity, in the following analysis we will mostly talk about $V_{out}(t)$.

Initially we concentrated our efforts on the Fourier transform and particularly the autospectrum of full and partial scans. These transforms had to be taken from the differentiated signal, V'_{out}, because the original signal contained a large dc component. This dc component, interpreted by the analyzer as a squarewave, completely dominated the spectrum and made an analysis of the more subtle differences very difficult. The analysis of the differentiated signal yielded clearer results. However, processing resulted in no improvement in the capability to detect a crack, compared with a direct analysis of V'_{out}. The reason for this failure lies in the nature of the background signal that has not yet been filtered out in V'_{out}--that is, it is not random. In fact, a high degree of repeatibility from measurement to measurement was found as long as the tuning conditions and the operating point of the

---

*In practice, the scanning velocity cannot be varied arbitrarily because of the built-in filters in the detector system.

detector remained unchanged. This fact prevents averaging of a large number of measurements in an attempt to cancel out the background signal. Averaging the autospectrum from measurements at different frequencies is not expected to alter that situation drastically for the same reasons (in addition, the present detector would require manual retuning for each new frequency, which would be very cumbersome).

Next, auto- and cross-correlation techniques were studied. When the two signals being compared are exactly the same, the cross-correlation function (CCF) becomes the autocorrelation function (ACF) $\Psi_{xx}(\tau)$.

Figure 26(a) shows the typical response V'_{out} for a crack on the "plug-type" shell D, and Figure 26(e) shows its ACF. The next few traces show various other portions of V'_{out} for the same shell and the CCF with the original reference signal as given in Figure 26(a). The signal given in 26(b) is also a crack-produced one. The CCF between the two signals shown in 26(f) exhibits a strong peak, indicating a high degree of similarity. The signal shown in 26(c) represents the response from a smaller pulse, and its CCF with the reference signal 26(g) clearly indicates a commonality. Finally, the CCF of the signals of 26(a) and 26(d) given in Figure 26(h) result in a peak of magnitude similar to that of the CCF of Figures 26(a) and 26(c). However, the signal of 26(d) represents no crack, which is clearly indicated by the single pulse present. If one were to establish a threshold level for the CCF between the response of a known crack and the signal to be tested, it is very likely that large single pulses of V'_{out} would be detected as cracks.

The reason for the failure of the CCF becomes clear from the reference signal and its ACF. The reference signal does not have a high enough signature (complexity) which would result in an ACF having pronounced but narrow pulses centered at $\tau = 0, \pm nT$, $n = 1, 2, \ldots$, and a value close to zero elsewhere. Because of this insufficient signature,

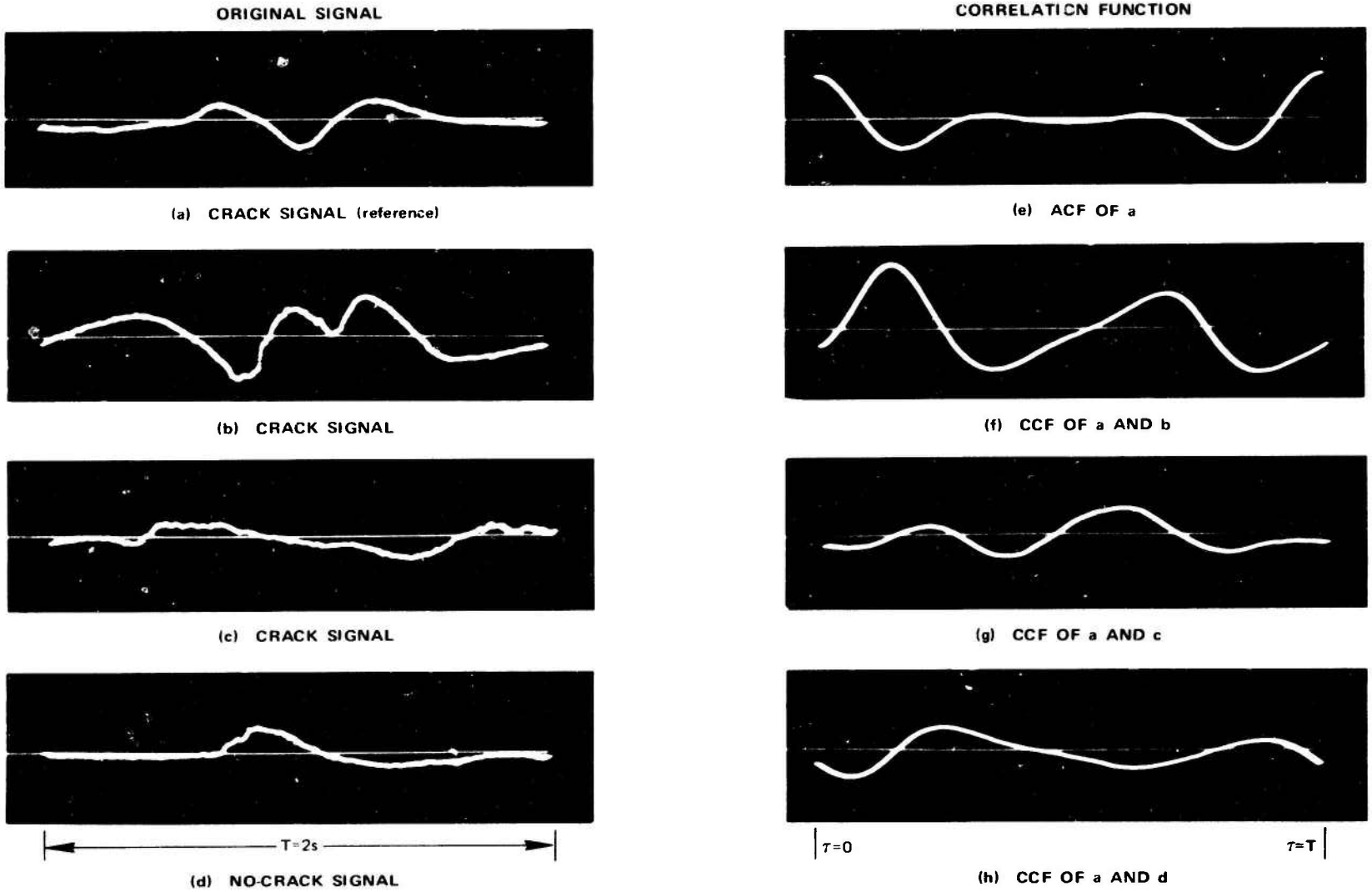

FIGURE 26 AUTO- AND CROSS-CORRELATION FUNCTIONS OF VARIOUS SEGMENTS OF V'_{OUT}

the CCFs between the reference signal and quite dissimilar but large signals are bigger than the CCFs between the reference signal and weak but very similar signals. Also, we know that a characteristic crack-produced signal that is uniform and could be used as a reference signal does not exist, making the detection problems even more difficult.

A rather simple method that could distinguish between a crack-produced response and a signal generated by a sudden change in the spacing between the detector and the specimen can be devised using digital logic circuitry. We know that crack-produced signals consist of at least a sequence of two pulses of opposite polarity. Their spacing in time is directly related to the detector geometry and the scanning velocity. This signal characteristic can lead to an automated crack-detection system that at this stage of the program would already have the capability of detecting cracks that are 1.5 mils wide, 5 mils deep, and 100 mils long, provided that the background signal can be kept at a level as low as 70 dB down from the even-mode signal, over a full scan.

VI CONCLUSIONS AND RECOMMENDATIONS

A. Summary of Results

A self-contained coupled-stripline crack-detector system was built, tested, and used for extensive measurements. Two different detectors were employed. Flat test plates were examined with a 4-inch-long planar detector. A curved detector for testing an 8-inch-long section of an 175-mm artillery-shell body in the tapered part of the shell was built. In this curved detector the coupled striplines were spiraled around the shell in a counterclockwise sense. If supplemented with a similar stripline system that is wound in the clockwise direction, cracks of any orientation could be detected. The stripline geometry proved to be relatively easy to construct and is easily adaptable to doubly curved surfaces with a rotational symmetry, as long as the radii are not too small.

The complete detector system consists of an RF part, which was built using almost exclusively commercial components, and a low-frequency electronics part that employs standard linear integrated circuits. System performance tests showed a close agreement between the calculations and the measurements. When the detector was applied to a shell and the system was properly tuned, a decoupling of the odd mode from the even mode of 75 dB or more was repeatedly obtained.

In operation we successfully detected cracks 0.0015 inch wide, 0.005 inch deep, and 0.100 inch long. A total of four shells and seven planar plates with more than 50 machined flaws were tested, all of which were detected by the present system. The recognition of crack-produced signals was facilitated by a logarithmic amplifier and an

analog differentiator in the low-frequency electronics. Any localized flaw is easily recognized by a series of pulse-pairs of alternating sign in the differentiated output signal. This signal would easily be amenable to an electronic detection scheme leading eventually to an automated system. The possibility for an automated system is one of the major assets of the stripline crack detector. Other advantages include the linear extension of the detector that allows the coverage of an area in one linear scan and the straightforward application of the detector to the test object (e.g., no immersion in a fluid required).

A remaining problem area of the present detector system is the so-called background signal. Small localized variations in the spacing between the detector and the test object lead to slowly varying changes in the output signal. This means a decrease in decoupling between the even and odd mode at the output of the detector, sometimes to levels as low as 35 dB. The result is reduced sensitivity with the possibility of failure to detect cracks of sizable dimensions. Several compensation schemes were discussed but rejected because they were found unsuitable. Toward the end of the contract a feedback system was conceived and some very preliminary tests have shown the feasibility of the idea. However, major design details remain to be worked out. The principle of the feedback system will be described briefly in the following.

If was found that the increase in decoupling during scanning was primarily due to a shift of the frequency of maximum decoupling, f_0, and not to the fact that the maximum decoupling itself decreased to a lower level. Measurements with the curved detector over a full scan indicated frequency shifts for f_0 of ±50 MHz, but variations in the maximum decoupling of less than 15 dB. The idea therefore was to build a feedback system that adjusts itself automatically to the frequency that results in the maximum decoupling (equal to minimum

background signal). A simplified schematic for this system is shown in Figure 27. A voltage-controlled oscillator feeds the detector system.

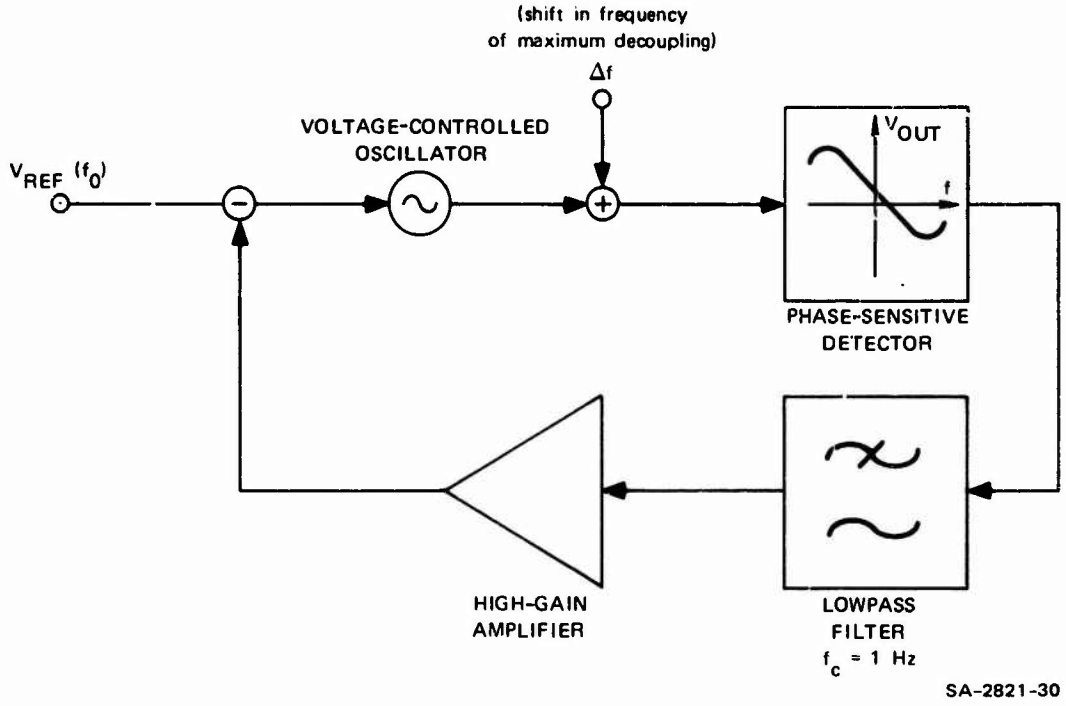

FIGURE 27 FEEDBACK SYSTEM TO MINIMIZE AND STABILIZE THE BACKGROUND SIGNAL

The shift in frequency due to the spacing variations is considered to be the error signal. A phase-sensitive detector measures the deviation of the output signal from zero (equal to infinite decoupling). This error signal is fed back into the oscillator and corrects the frequency of the oscillator until maximum decoupling is obtained. Initially f_0 is adjusted by means of a reference voltage, V_{ref}, for maximum decoupling. The low-pass filter in the feedback loop restricts the regulation to slow changes (background signal) but not to crack-produced changes. Therefore, the output signal of the phase-sensitive detector would directly indicate cracks.

Preliminary measurements on such a feedback system look very promising. Stabilization was achieved in a number of cases. In those cases, the output signal was essentially flat at a decoupling level of 68 dB and all four cracks of Shell D were detected. The system is far from being operative and therefore is not included in the main technical description. However it appears to be the most promising area for future improvements, because it offers a solution to the problem of the changing sensitivity and the chance of "losing" a crack, which are the most significant deficiencies of the present system.

Finally, various signal-processing techniques were investigated. The autocorrelation and cross-correlation functions of samples of the output signal and the response of a known crack were calculated, using a modern time-series analyzer. It was found that no improvement in detectability over a visual inspection was possible. The reason for this failure lies in the low signature (complexity) of a crack-produced signal compared with a signal of non-crack origin--e.g., noise. Detectors with more than two striplines (e.g., four to six) could lead to crack-produced signals of a more distinct signature.* But the larger size of a multistrip detector in the scanning direction bears an increased risk that closely spaced cracks produce overlapping responses that would be difficult to separate. Therefore, the largely increased circuit complexity and the problem of overlapping responses from separate cracks seem not to favor a multistrip detector, even though from a

---

*The present problem is similar to the transmission of coded digital information. There, each bit of information is transmitted as a sequence of pulses. The optimum code has an autocorrelation function with the narrowest pulsewidth at $\tau = 0$, and with the lowest sidelobe level for a given length of the code (see, e.g., Cook and Bernfield[9]).

theoretical point of view such a solution appears to offer advantages for signal-processing purposes.

B. Recommendations

Further improvement of the present system is required in order to make it a mature instrument for detecting cracks in metal surfaces. Some possible refinements have been discussed in previous parts of this report. In the following the most promising areas for improvements and extensions of the existing work are listed in order of descending priority.

(1) Most important would be the implementation of a feedback system as discussed in the previous section. Initially, it is expected that the existing design could be modified to incorporate the feedback system. This improvement should solve the sensitivity problems of the present system. It would stabilize the background signal at a low level and guarantee that cracks larger than a minimum size will be detected, unless they are in parallel with the striplines.

(2) In order to detect a crack of any orientation and to detect the exact location of a crack, a system consisting of two orthogonal striplines is required. With the exception of a few components that could be shared between the two systems, this would involve duplication of the existing system. If mere knowledge of the existence of cracks is required, then the output signals of the two detectors could be processed separately. However, if the location of a crack is also important, then the two outputs have to be compared with each other. With only one crack present, the location can be determined exactly. For two or more cracks detected during a full scan the result will be ambiguous, and a different technique would be required to determine the location uniquely.

(3) Operation at a higher frequency (e.g., 30 GHz) will improve the sensitivity, because the response of a crack of a given size is directly proportional to frequency [see Eq. (10)]. However, a stripline construction at 30 GHz would be combined with increased technological difficulties. Alternatively, a detector using transmission lines other than striplines (e.g., waveguides) could be used. In any case, a detailed study would be required to determine the impacts of a change in frequency.

(4) Systems with multiple striplines could be examined as discussed above. The advantage of a multistrip system would lie in the improved ability to distinguish a crack from noise. But, it does not solve the basic problem of the background signal and therefore the impaired sensitivity of the detector. A multistrip detector would be useful only in conjunction with a system that solves the sensitivity problem--e.g., with the proposed feedback network.

Among the four proposed improvements, the first two are considered essential and would enhance the practical usefulness of the instrument. The other two are of lesser significance but might be considered for further refinements.

Appendix

LOW-FREQUENCY ELECTRONIC CIRCUIT DIAGRAMS

Appendix

LOW-FREQUENCY ELECTRONIC CIRCUIT DIAGRAMS

Figures A-1 through A-5 show circuit diagrams of all electronic circuits that were built for the crack-detector system. All designs are well known and are described in the National Semiconductor Application Notes.[10]

Preceding page blank

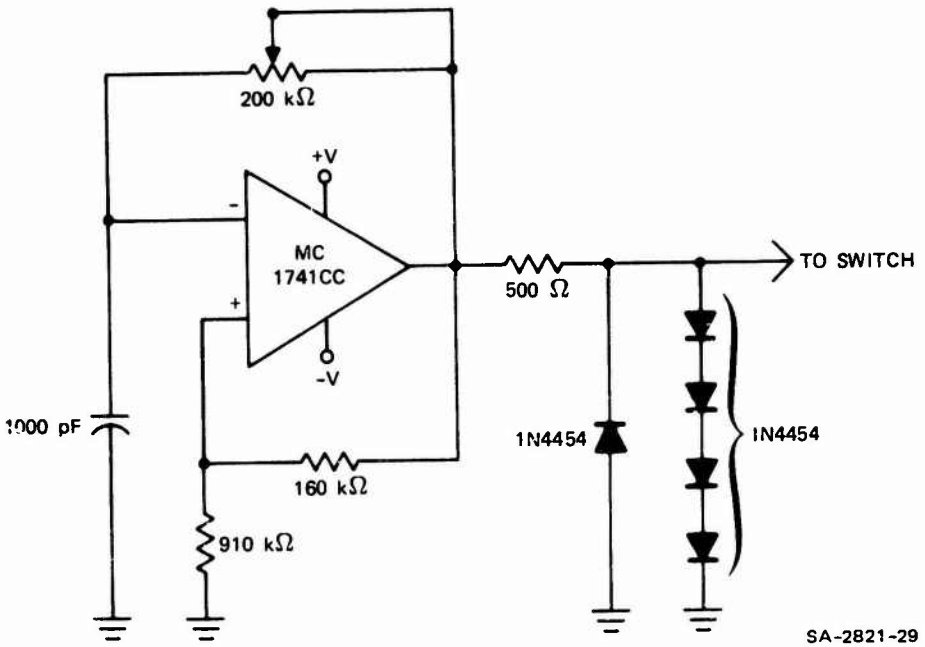

FIGURE A-1 1-kHz SQUARE-WAVE OSCILLATOR

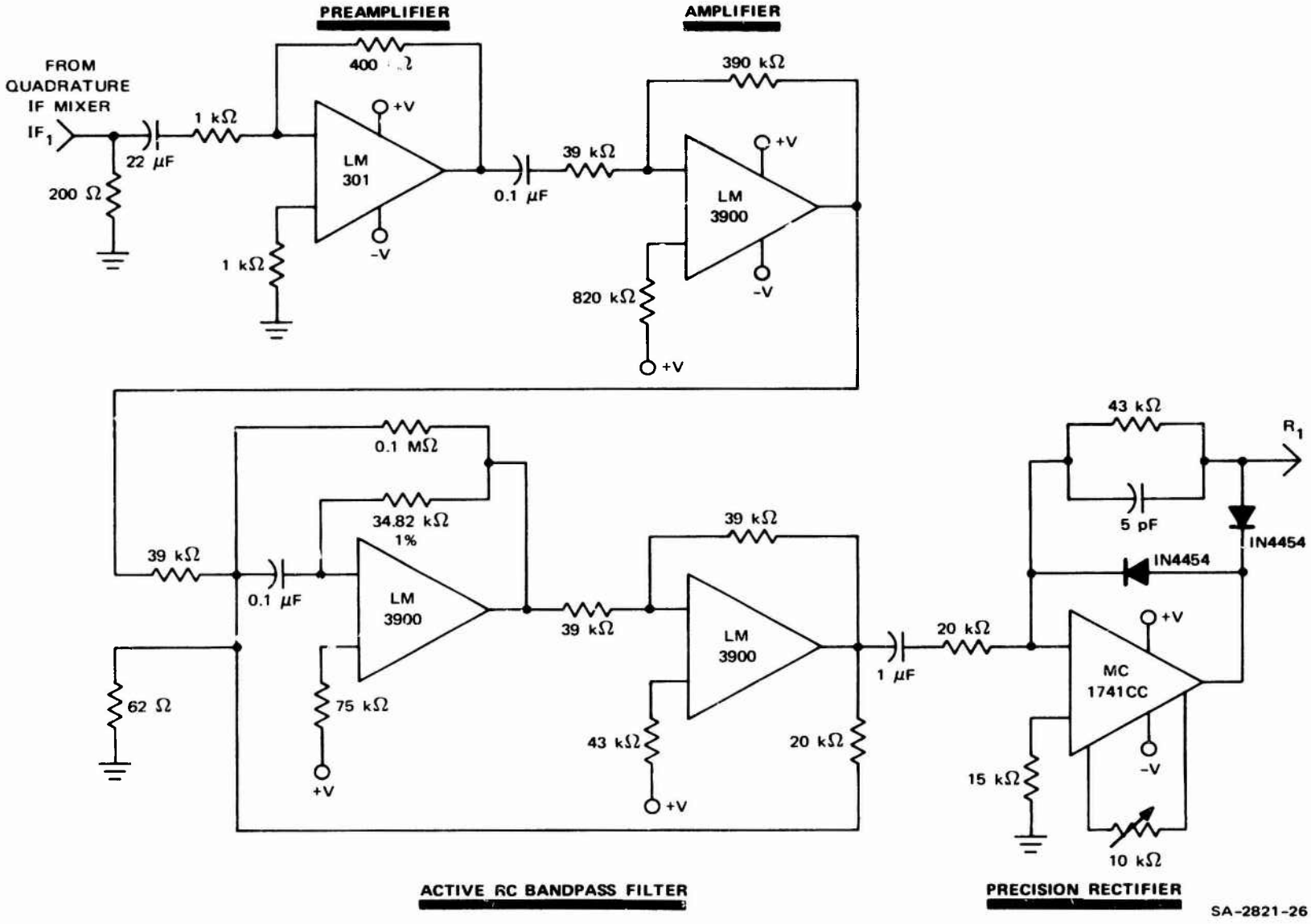

FIGURE A-2 PREAMPLIFIER 1-kHz BANDPASS FILTER AND PRECISION RECTIFIER (one of two units)

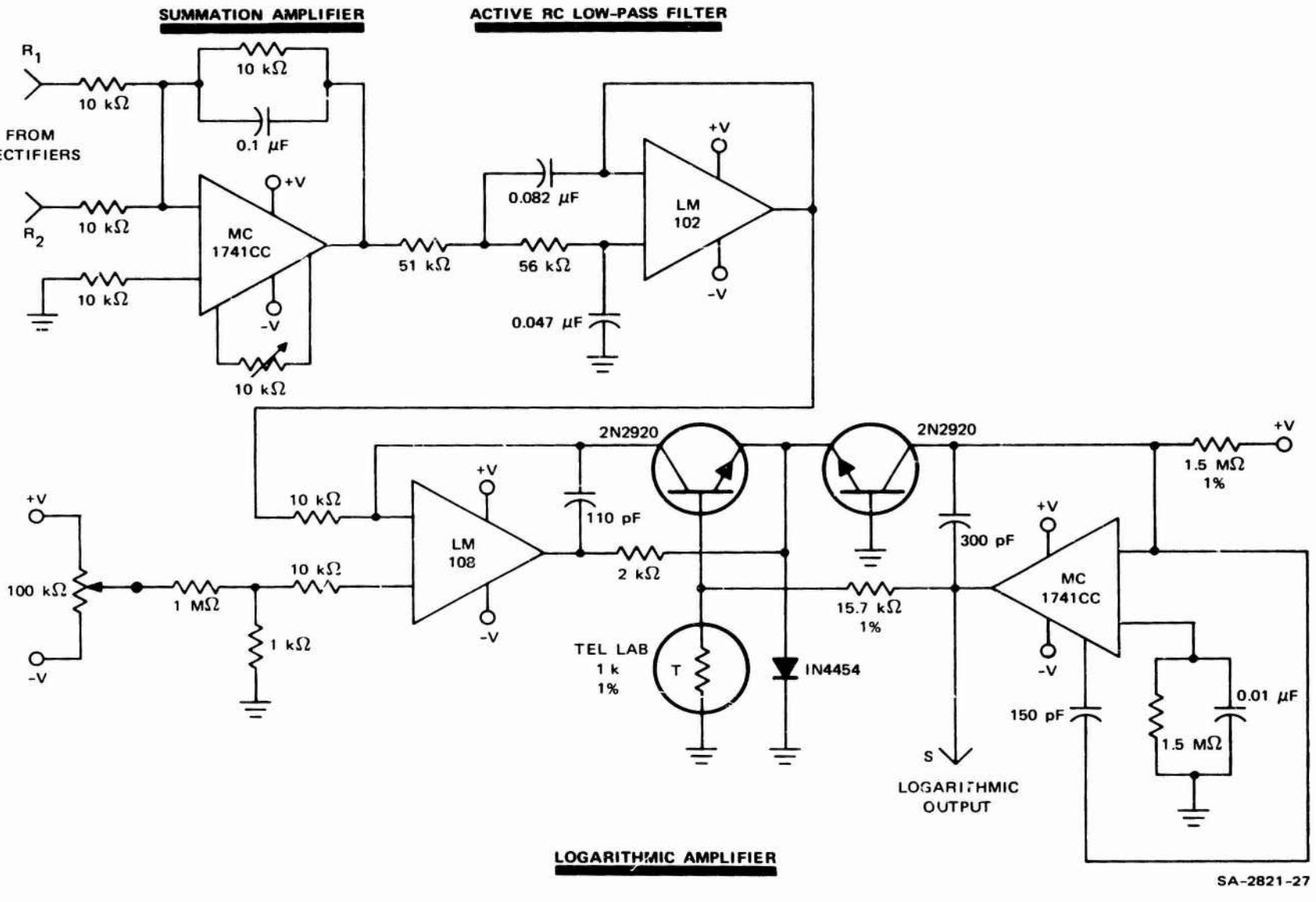

FIGURE A-3 SUMMATION AMPLIFIER, LOW-PASS FILTER, AND LOGARITHMIC CONVERTER

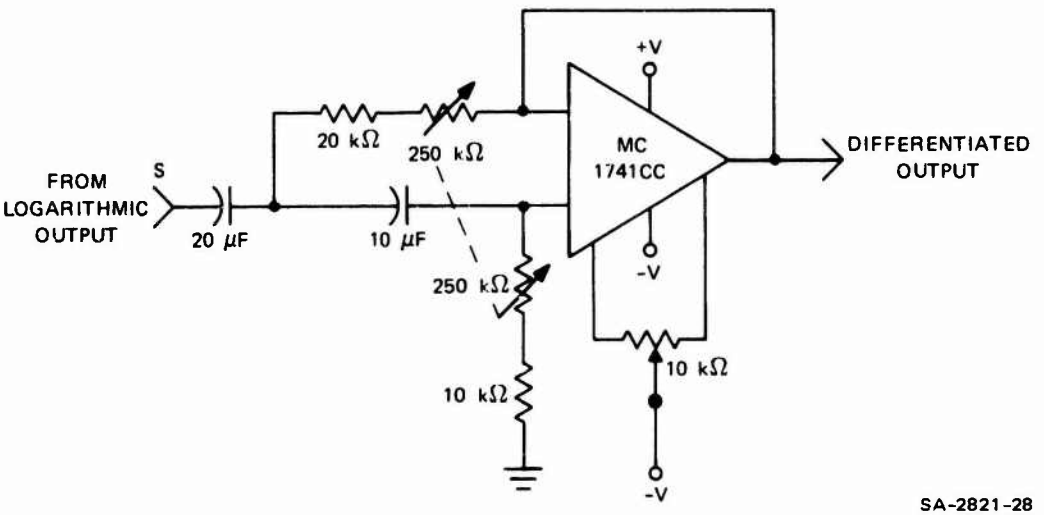

FIGURE A-4 ACTIVE HIGH-PASS FILTER WITH VARIABLE CUTOFF FREQUENCY

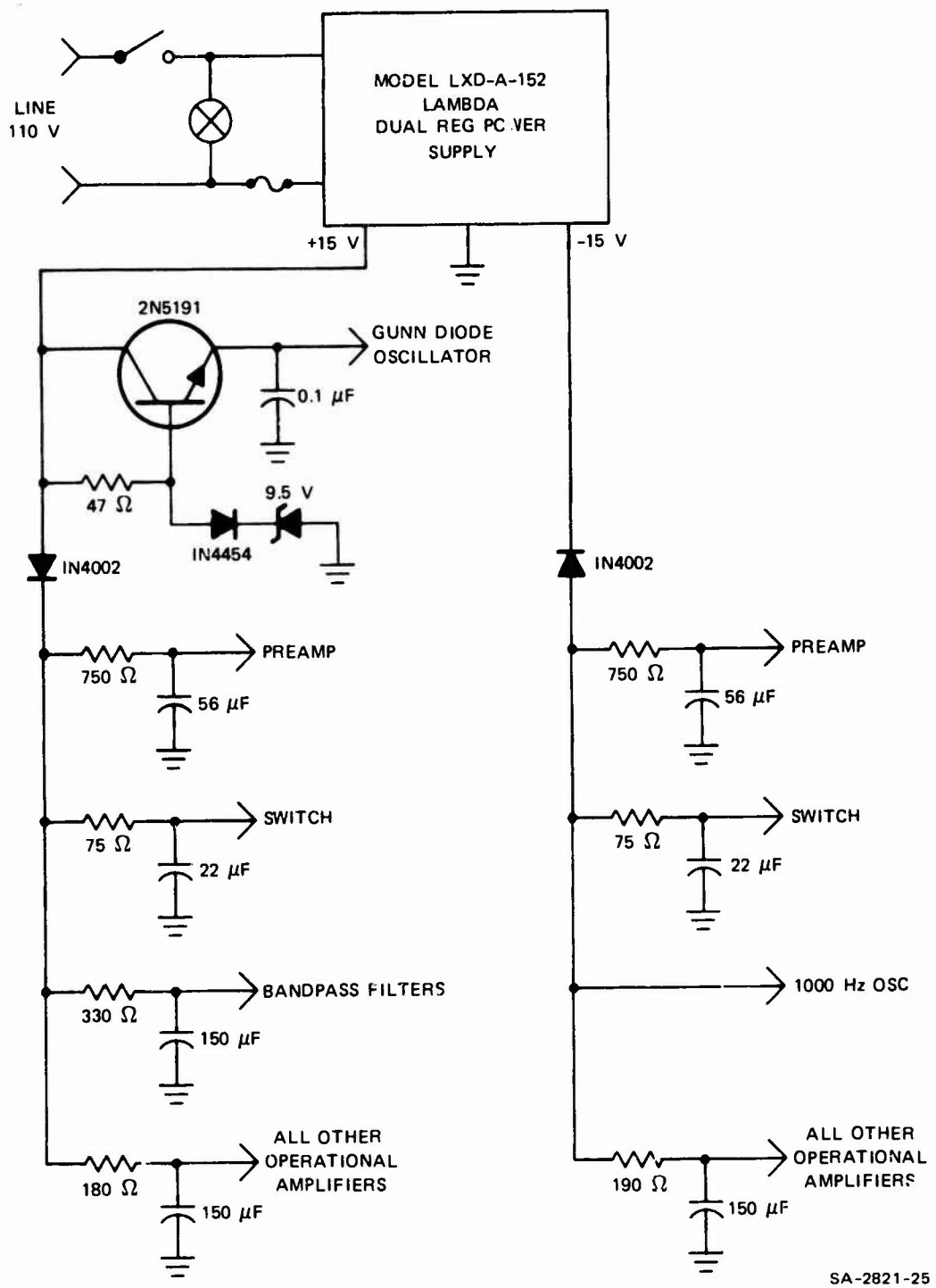

FIGURE A-5 dc POWER SUPPLY

REFERENCES

1. R.J. Hruby and L. Feinstein, "A Novel Nondestructive, Noncontacting Method of Measuring the Depth of Thin Slits and Cracks in Metals," Rev. Sci. Inst., Vol. 41, No. 5, pp. 679-683 (May 1970).

2. L.A. Robinson and U.H. Gysel, "Microwave Coupled Stripline Surface Crack Detector," Final Report, Contract DAAG46-72-C-0019, SRI Project 1490, Stanford Research Institute, Menlo Park, California (August 1972).

3. G.L. Matthaei, L. Young, and E.M.T. Jones, Microwave Filters, Impedance Matching Networks, and Coupling Structures, Fig. 5.05-2(a) (McGraw-Hill Book Co., New York, N.Y., 1964).

4. H.A. Bethe, "Theory of Diffraction by Small Holes," Phys. Rev., Vol. 66, Nos. 7 and 8, pp. 163-182 (1 and 15 October 1944).

5. R. Levy, "Analysis and Synthesis of Waveguide Multiaperture Directional Couplers," IEEE Trans. Microwave Theory and Techniques, Vol. MTT-16, No. 12, pp. 995-1006 (December 1968).

6. S.B. Cohn, "Shielded Coupled-Strip Transmission Line," IRE Trans., Vol. MTT-3, pp. 29-38, Fig. 2(e) (October 1955).

7. S. Ramo and J.R. Whinnery, Fields and Waves in Modern Radio, Secs. 8.04-8.11 (John Wiley and Sons, Inc., New York, N.Y., 1953).

8. F.H. Lange, Correlation Techniques (D. van Nostrand, Princeton, N.J., 1968).

9. C.E. Cook and M. Bernfeld, Radar Signals, Chapter 8 (Academic Press, New York, N.Y., 1967).

10. Linear Applications, National Semiconductor Corporation, Santa Clara, California (1973).